Desalination 634 (2026) 120291

Contents lists available at ScienceDirect

Desalination

journal homepage: www.elsevier.com/locate/desal

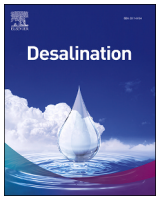

Efficient nutrient recovery from source-separated urine via a hybrid Membrane Bioreactor and Electrodialysis (MBR-ED) system

Hanwei Yu [a], Weonjung Sohn [a], Sherub Phuntsho [a], Youngjin Kim [b], June-Seok Choi [c], Jong-Hun Lee [c], Youngkwon Choi [c], Ho Kyong Shon [a,*]

[a] ARC Research Hub for Nutrients in a Circular Economy, Center for Technology in Water and Wastewater, School of Civil and Environmental Engineering, Faculty of Engineering and IT, University of Technology Sydney, P.O. Box 123, Broadway, NSW, 2007, Australia
[b] Department of Environmental Engineering, Korea University, 2511, Sejong-ro, Sejong-si, 30019, Republic of Korea
[c] Department of Civil, Environmental and Architectural Engineering, Korea University, 145 Anam-ro, Seongbuk-gu, Seoul, 02841, Republic of Korea

HIGHLIGHTS

- A hybrid MBR-ED system enabled efficient nutrient recovery and concentration from source-separated human urine.
- pH governed ion transport behavior, enabling higher monovalent nutrient concentration and energy efficiency under near-neutral ED operation.
- ED reduced nutrient-normalized energy consumption by one to two orders of magnitude compared with thermal distillation.
- The integrated process offers a compact, low-energy, and scalable pathway for circular fertilizer production.

GRAPHICAL ABSTRACT

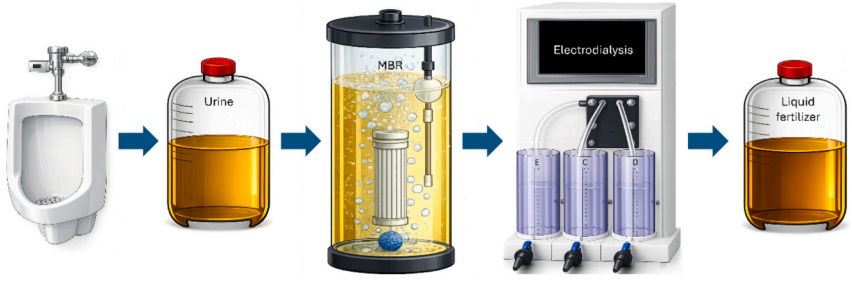

ARTICLE INFO

Keywords:
Nutrient recovery
Electrodialysis
Membrane bioreactor
Circular economy
Urine valorisation
Sustainable fertilizer production

ABSTRACT

Nutrient recovery from source-separated human urine represents a promising pathway for sustainable fertilizer production within a circular economy framework. In this study, a hybrid membrane-based system integrating a membrane bioreactor (MBR) and electrodialysis (ED) was developed for efficient recovery and concentration of inorganic nutrients (N, P, and K). Hydrolyzed urine was first treated using an aerobic MBR to stabilize nitrogen and reduce organic content, producing a permeate with a stable ionic composition suitable for downstream electrochemical processing. The MBR permeate was subsequently concentrated by ED under acidic and near-neutral operating conditions. High removal efficiencies of 91–98% for nitrate, 89–97% for ammonium, and 87–97% for potassium were achieved in the diluate compartment. Under near-neutral conditions, final concentration factors reached 10.8 for potassium, 10.3 for ammonium, and 9.3 for nitrate, corresponding to a 9.2-fold increase in TDS. Solution pH plays a critical role in governing ion transport behavior, with near-neutral operation enabling higher final enrichment of monovalent nutrient ions. Compared with conventional thermal distillation, ED reduced apparent nutrient-normalized specific energy consumption from 626 to 8.5 kWh/kg for potassium, from 306 to 12.6 kWh/kg for ammonium, from 291 to 19.3 kWh/kg for nitrate, and from 5321 to 358.9 kWh/kg for phosphate, representing one to two orders of magnitude improvement in energy efficiency. These results demonstrate that functional integration of MBR conditioning and ED concentration enables high-

* Corresponding author.
E-mail address: Hokyong.Shon-1@uts.edu.au (H.K. Shon).

https://doi.org/10.1016/j.desal.2026.120291
Received 27 February 2026; Received in revised form 8 May 2026; Accepted 10 May 2026
Available online 12 May 2026

degree nutrient enrichment with substantially lower energy demand, highlighting the potential of integrated membrane processes for decentralized urine valorization and circular fertilizer production.

1. Introduction

Human urine is a concentrated nutrient source that contributes approximately 85–90% of the nitrogen, 50–80% of the phosphorus, and 80–90% of the potassium in domestic wastewater, despite accounting for only about 1% of its total volume [1–6]. As a result, nutrient recovery from urine has been recognized as a paradigm shift toward sustainable nutrient management [2,6–9]. Source separation of urine at the point of generation allows efficient nutrient recovery while substantially reducing nutrient loads in municipal wastewater treatment plants, thereby decreasing aeration energy demand by up to 33% and direct CO_2 emissions by roughly 25% [3,10]. Several countries, including the United States, Australia, Switzerland, South Africa, and Ethiopia, have initiated large-scale programs to collect and valorize source-separated urine within circular economy frameworks [3,4,11].

The key challenges of the direct agricultural use of urine, such as unpleasant odors, high organic content, and ammonia volatilization due to high pH, have led to increased attention on various urine treatment technologies [4,12,13]. Various technologies have been investigated for nutrient recovery, such as chemical precipitation, adsorption, and evaporation, but these typically require substantial chemical inputs, entail high energy consumption, and provide limited removal of micropollutants [5,6,14–20]. Membrane-based processes, in contrast, have emerged as promising alternatives for treating source-separated urine, offering simultaneous organic removal, volume reduction, and micropollutant rejection with relatively low energy demand [21–24]. Biological nitrification within membrane bioreactors (MBRs) has proven particularly effective for stabilizing volatile ammonia into nitrate and for eliminating odor-causing organics, yielding a safe, odor-free liquid fertilizer [3,13,25–29]. Although the MBR process effectively stabilizes nutrients and removes organics, the resulting permeate remains dilute and requires further concentration obtain a nutrient-rich product suitable for storage, transportation, and commercial fertilizer production [13,25,29]. Conventional concentration methods, such as thermal evaporation and distillation, are energy-intensive and may cause nutrient loss or thermal degradation [23,30–32]. Moreover, these processes demand long operation times and are unsuitable for decentralized applications where compactness and energy efficiency are critical.

Electrodialysis (ED) has emerged as an attractive non-thermal alternative for nutrient concentration, operating under mild conditions with lower energy consumption [33–39]. Driven by an applied electric field, ED selectively transports ions through ion-exchange membranes, enabling simultaneous separation and concentration of dissolved nutrients without the addition of chemicals [7,38,40–42]. Compared to conventional methods, ED offers higher selectivity, controllable ion transport, and minimal volatilization loss of nitrogen compounds [1,38,43,44]. These advantages make it particularly suitable for concentrating pretreated urine into a nutrient-rich fertilizer solution while maintaining chemical stability and product quality [40,45,46]. Previous studies have demonstrated the feasibility of ED for nutrient recovery and concentration from a wide range of wastewater and waste-derived streams, including municipal wastewater effluents, anaerobic digestate, centrate, liquid digestate, and fermented wastewaters [47–58]. ED has been shown to effectively concentrate major nutrient ions such as ammonium, nitrate, potassium, and phosphate, while simultaneously producing a low-salinity diluate suitable for water reuse [43,47,49,53,59–62]. This applicability has also been extended to urine-derived streams. For example, De Paepe et al. reported that ED treating nitrified urine achieved concentration factors of 4.3 for nitrate, 2.6 for phosphate, and 4.6 for potassium [45].

Despite these advances, integrated process design that couples biological stabilization with high-degree electrochemical concentration under controlled operating strategies remains comparatively underexplored. Coupling MBR and ED processes offers a promising route providing an energy-efficient and environmentally friendly pathway for comprehensive nutrient recovery. This functional integration, in which the aerobic MBR serves primarily as a biological conditioning step to stabilize nitrogen species and reduce organic content, thereby generating a low-fouling permeate suitable for subsequent electrochemical process [3,13,39], while ED subsequently acts as the core concentration unit, enabling progressive nutrient enrichment through a fixed feed concentration strategy. In this study, such a hybrid MBR-ED system was developed and systematically evaluated for inorganic nutrient recovery and concentrated liquid fertilizer production from source-separated urine. ED was investigated under both acidic and near-neutral conditions to elucidate the influence of pH on ion transport behavior, concentration efficiency, and energy consumption. Furthermore, ED performance was benchmarked against thermal distillation to assess relative energy efficiency. Through this integrated and controlled approach, this work demonstrates efficient nutrient concentration with substantially reduced energy consumption, highlighting the potential of integrated membrane processes for decentralized sanitation and circular nutrient recovery applications.

2. Experimental

Fig. 1 illustrates the overall configuration and workflow of the hybrid MBR-ED system developed in this study for nutrient recovery and liquid fertilizer production from source-separated human urine. The system integrates biological stabilization and nitrification with electrochemical concentration in a sequential manner. The MBR was operated to provide a biologically stabilized and low-organic feed suitable for subsequent electrochemical concentration [3,13,39,63], whereas ED was responsible for achieving progressive nutrient enrichment. Source-separated urine was first treated in an aerobic MBR to reduce organic matter and convert ammoniacal nitrogen into oxidized nitrogen species, producing a stable, low-organic permeate with a well-defined ionic composition [3,13]. The MBR permeate was subsequently processed by a lab-scale ED unit, in which inorganic nutrients were progressively concentrated using a fixed feed concentration strategy to generate a nutrient-rich liquid fertilizer, while producing a low-salinity diluate stream.

2.1. MBR setup and nitrification operation

Source-separated urine used in this study was collected from Building 11 at the University of Technology Sydney (UTS), which is equipped with urine-diverting sanitation facilities. The building incorporates waterless urinals connected to dedicated urine collection pipelines on each floor, allowing undiluted urine to be conveyed to a centralized storage tank with a capacity of approximately 100 L located in the basement. When required for laboratory experiments, the stored urine was transported to a pilot-scale MBR. The detailed physicochemical characteristics of the collected urine have been reported in our previous publication [3,13]. Due to prolonged storage prior to use, the urine was fully hydrolysed, with urea completely converted and no residual urea remaining at the time of feeding. The MBR employed in this study had been operated under steady-state nitrifying conditions for an extended period before the commencement of the present experiments. Reactor start-up, biomass acclimation, and long-term operational stability have been comprehensively described in our previous work [3,13,63]. Briefly, the reactor was inoculated with activated sludge sourced from

the Central Park decentralized wastewater treatment facility (Ultimo, NSW, Australia), followed by gradual acclimation to urine treatment and nitrification. As a result, a stable and resilient nitrifying microbial community was established and maintained throughout the experimental campaign.

During operation, the hydrolysed urine was continuously introduced into the MBR using an automated pH-controlled dosing pump (BL7916–1, Hanna Instruments, Australia). This system provided both feed delivery and alkalinity supplementation, enabling precise regulation of reactor pH at 6.1. Maintaining appropriate pH is essential for nitrification, as it controls the speciation balance between NH_4^+/NH_3 and HNO_2/NO_2^-, which directly affects the activity and kinetics of ammonia-oxidizing bacteria (AOB) and nitrite-oxidizing bacteria (NOB). Effective pH control promotes complete nitrification while suppressing nitrite accumulation, which is undesirable for downstream fertilizer reuse due to its potential phytotoxic effects. Biomass retention and solid-liquid separation were achieved using a commercial polyvinylidene fluoride (PVDF) hollow-fibre microfiltration membrane module (Beijing OriginWater Technology, China). The membrane featured a nominal pore size of 0.1 μm, inner and outer fibre diameters of 0.95 mm and 2.0 mm, respectively, and an effective surface area of 0.06 m^2. A level sensor installed on the reactor wall functioned as a water-level controller, maintaining a constant hydraulic head across the membrane to ensure stable and reproducible permeate flux. Aeration was supplied via ceramic diffusers connected to an air pump at a flow rate of 0.2 m^3/h, ensuring sufficient oxygen transfer for biological oxidation. Under these conditions, dissolved oxygen concentrations were consistently maintained above 6 mg/L, supporting complete conversion of ammoniacal nitrogen to nitrate. The resulting MBR permeate exhibited low organic content and a stable ionic composition, making it suitable for subsequent nutrient concentration by ED.

2.2. ED setup and liquid fertilizer concentration

Fig. 2 illustrates the working principle and ion transport mechanisms of ED used for nutrient concentration. The ED stack consists of alternating cation-exchange membranes (CEMs) and anion-exchange membranes (AEMs) positioned between an anode and a cathode, forming a series of diluate and concentrate compartments [1,38,57]. Under an applied electric field, cations migrate toward the cathode and selectively pass through CEMs while being rejected by AEMs. Conversely, anions migrate toward the anode and permeate through AEMs while being blocked by CEMs. As a result, ionic species are continuously transported from the diluate compartments into the adjacent concentrate compartments, leading to ion depletion in the diluate stream and enrichment in the concentrate stream [38,43,47,64,65]. Organic compounds and other non-ionic or weakly charged species are largely retained in the diluate compartments due to size exclusion and limited electro-migration, thereby minimizing their accumulation in the concentrate stream.

In this study, a lab-scale ED system (model EX-3BT, HZ Lanran) equipped with 10 pairs of Ionsep® cation- and anion- exchange membranes was employed for liquid fertilizer concentration. Each membrane had an effective area of 55 cm^2, a thickness of approximately 0.5 mm, an area resistance of $\leq$9.0 Ω·cm^2 in 0.5 N NaCl, and an operational pH range of 2–10. The ED concentration experiment was conducted using a fixed feed concentration strategy to concentrate the urine-derived feed solutions under both acidic and near-neutral pH conditions, characterized by an initial conductivity ranging from 32 to 36 mS/cm. The operation parameters were set with an upper voltage limit of 15 V and an upper current limit of 1.1 A, with each cycle operated for 30 min and terminated when the end-cycle current decreased to $\leq$0.5 A.

Initially, 500 mL of feed solution was introduced into the dilute compartment, while 500 mL of deionized (DI) water was added to the concentrate compartment. The electrode rinsing compartments were filled with 500 mL of 3% Na_2SO_4 solution to ensure adequate ionic conductivity and electrochemical stability. After each cycle, the dilute compartment was replenished with fresh feed solution while the concentrate and electrode rinsing compartments remained unchanged. This process was repeated until the marginal energy consumption per unit increase in conductivity in the concentrate compartment reached a

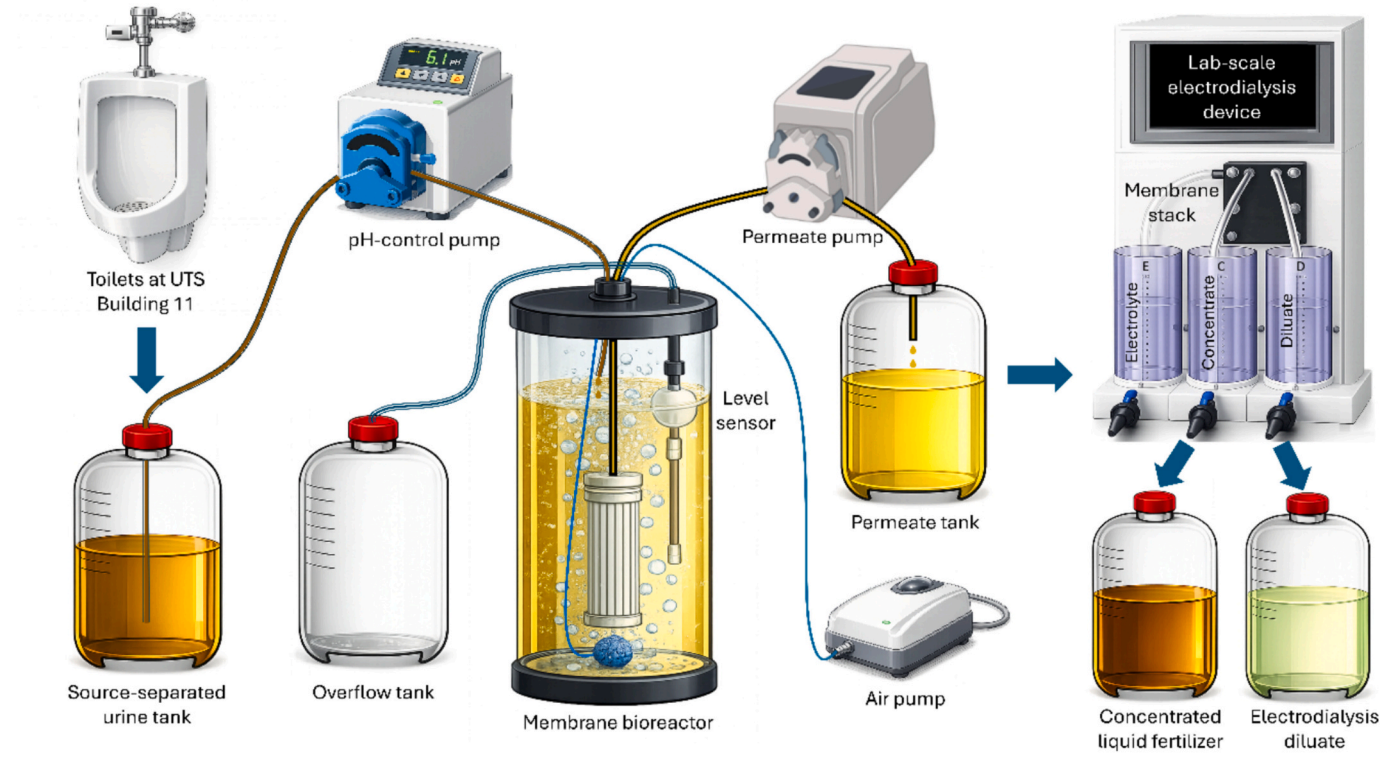

Fig. 1. Schematic process of the MBR-ED system for nutrient recovery from source-separated urine.

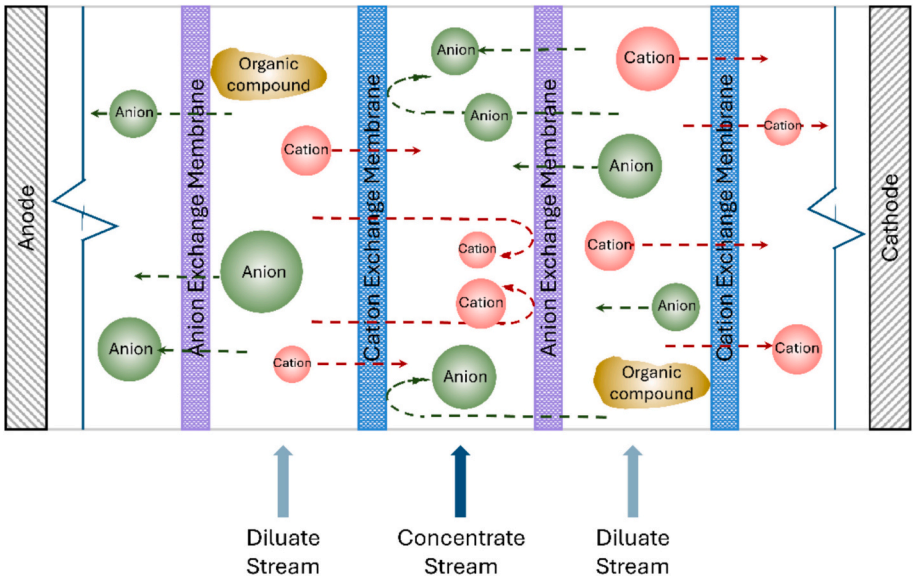

Fig. 2. Schematic illustration of ED process and ion transport mechanisms for nutrient concentration.

predefined threshold. Finally, a total of 18 cycles and 20 cycles were conducted under acidic and near-neutral conditions, respectively. To mitigate potential membrane fouling and scaling during prolonged operation, periodic membrane rinsing was implemented as a preventive measure. During each rinsing event, the diluate and concentrate compartments were drained and refilled with DI water, after which the circulation pump was activated for 5 min to flush the membranes. This rinsing procedure was repeated three times per event. It should be noted that no visible membrane fouling or significant deterioration in electrical performance was observed during the concentration experiments. The rinsing protocol was therefore adopted as a precautionary strategy to maintain stable long-term operation. Following rinsing, the ED process was resumed in the subsequent concentration cycle. After each concentration cycle, around 20 mL of liquid samples were collected from both the diluate and concentrate compartments for ion concentration analysis.

2.3. Analytical methods

The concentrations of soluble metal cations, including sodium, potassium, magnesium, and calcium, were quantified using inductively coupled plasma mass spectrometry (ICP-MS; Agilent 7900, Agilent Technologies, USA). Nitrogen species, including ammonium nitrogen (NH_4^+-N) and nitrate nitrogen (NO_3^--N), as well as phosphate (PO_4^{3-}-P) and other major anions such as sulfate (SO_4^{2-}) and chloride (Cl^-), were analyzed using standard colorimetric test kits (Merck Millipore, USA). Absorbance measurements were performed on a spectrophotometer (Spectroquant NOVA 60, Merck, Germany) to determine analyte concentrations. Total organic carbon (TOC) was measured using a TOC analyzer (multi N/C 2000, Analytik Jena, Germany). Conductivity, total dissolved solids (TDS), and pH were monitored using a multi-parameter meter. Electrical parameters, including current, voltage, cumulative charge transfer, and total energy consumption during ED operation, were continuously recorded by the EX-3BT ED system. The ED experiments were conducted as continuous cycle-based operations, and the reported results represent the temporal evolution of system performance within a single representative long-cycle experimental sequence rather than averages from independent repeated runs. Due to minor batch-to-batch variations in the feed composition, repeating full long-cycle experiments would introduce additional variability. Therefore, representative runs were used to ensure consistent initial conditions and reliable interpretation of system performance. Ion concentrations measured by ICP-MS were obtained under stable instrument conditions, ensuring high analytical precision. For colorimetric and physicochemical analyses, duplicate or triplicate measurements were performed, and the variation among replicates was within ±5%, confirming good analytical reproducibility. Error bars are not presented in the figures, as the observed variations were small and did not affect the overall trends.

ED performance was evaluated using concentration factors, ion removal percentages, and specific energy consumption metrics. The concentration factor for each ion or physicochemical parameter was calculated to quantify the degree of enrichment achieved in the concentrate compartment:

$$CF_i = \frac{C_{i,conc}}{C_{i,\ feed}}$$

where $C_{i,conc}$ is the concentration of species i in the concentrate compartment at the end of each ED cycle operation, and $C_{i,feed}$ is its concentration in the feed solutions. For conductivity- and TDS-based concentration factors, the same formulation was applied using the corresponding measured values. Ion removal performance in the diluate compartment was quantified on a per-cycle basis using the removal efficiency:

$$Removal\ efficiency = \left(1 - \frac{C_{i,dil,end}}{C_{i,\ feed}}\right) \times 100\%$$

where $C_{i,dil,end}$ is the concentration measured in the diluate compartment at the end of that cycle. This definition reflects the fixed feed concentration strategy employed, in which the diluate compartment was replenished with fresh feed solution at the start of each cycle. The apparent current efficiency (CE) was calculated to evaluate the effectiveness of electrical current utilization for ion transport. CE was determined based on Faraday's law as:

$$CE = \frac{z_i F \sum \Delta n_i}{\sum Q}$$

$$\Delta n_i = \frac{(C_{i,feed} - C_{i,dil,end})V}{M_{i.}}$$

where z_i is the ionic charge of the ion i, F is the Faraday constant (96,485C/mol), Δn_i is the number of moles of ion i transported from the diluate to the concentrate, V is the solution volume, M_i is the molar mass of the ion i, and Q is the total electric charge passed, calculated from the

time integration of the applied current. To enable direct comparison between ED- and distillation-based concentration processes, a normalized specific energy consumption for nutrient concentration was calculated as:

$$SEC@nutrient = \frac{E}{m_i}$$

where E is the total energy consumption associated with nutrient concentration and m_i is the net mass of the target nutrient i accumulated in the concentrate. SEC values were reported individually for potassium, ammonium, nitrate, and phosphate to reflect nutrient-specific concentration efficiency. It should be noted that, in this multi-ion system, the calculated CE and SEC reflect the apparent current efficiency and specific energy consumption for each target ion, as the total applied current and energy consumption are shared among multiple competing ions and may also be affected by co-ion leakage and non-ideal membrane permselectivity.

3. Results and discussion

3.1. MBR permeate characteristics

Hydrolyzed urine was first treated using a MBR to remove organic matter and stabilize nitrogen species, producing an MBR permeate that served as the baseline nutrient solution for subsequent concentration experiments. The ionic composition of the MBR permeate is summarized in Table 1. The permeate exhibited a conductivity of 23.5 mS/cm and a TDS concentration of 15.98 g/L, confirming that urine-derived nutrients remained highly concentrated after biological treatment. Nitrogen was present mainly as ammonium and nitrate, with concentrations of 1907 and 1826 mg/L, respectively, while potassium and sodium were the dominant cations at 996 and 1190 mg/L. Phosphate and sulfate were also present at appreciable levels, indicating the suitability of the MBR permeate as a nutrient-rich feed for downstream concentration.

To establish a benchmark for energy consumption comparison with ED, the MBR permeate was first concentrated using thermal distillation. The distillation concentrate was subsequently diluted approximately tenfold with DI water to generate a processed MBR permeate with controlled composition and conductivity. This solution served as the feed for ED experiments under both acidic and near-neutral conditions. Specifically, it was used directly for acidic operation, while for near-neutral experiments, the same solution was further adjusted to pH of 6.5 using potassium hydroxide. This approach ensured that the feed solution used for ED experiments had a reproducible ionic matrix while allowing a direct comparison between ED- and distillation-based concentration processes in terms of energy efficiency. The processed MBR permeate showed an increased conductivity of 33–37 mS/cm and a TDS concentration of 20–23 g/L. Because the physicochemical characteristics of the MBR permeate exhibited minor batch-to-batch fluctuations, the processed MBR permeate used for ED experiments showed mild variations in composition, which are documented in the corresponding tables in each results section.

3.2. ED concentration performance under acidic conditions

Under acidic operating conditions, ED was performed using a fixed feed concentration strategy to evaluate the concentration performance of the processed MBR permeate. Prior to ED treatment, the MBR permeate was concentrated by distillation and subsequently diluted with DI water to obtain the processed MBR permeate used as the ED feed under acidic conditions, without further pH adjustment. The physicochemical characteristics of the processed MBR permeate are summarized in Table 2. Using this feed solution, a total of 18 consecutive ED concentration cycles were conducted to progressively transfer ions from the diluate compartment to the concentrate compartment.

Fig. 3A presents the evolution of output current, voltage, and calculated stack resistance over the 18 ED concentration cycles. In Cycle 1, the electrical response exhibited a distinct three-stage behavior. At the beginning of the cycle, the output voltage rapidly increased to the preset upper limit of 15 V, while the output current remained low and the calculated resistance was high. As the cycle progressed, the current gradually increased toward the preset limit, accompanied by a slight decrease in operating voltage and a corresponding decrease in stack resistance. Toward the end of Cycle 1, the voltage again reached the upper limit, while the current declined and the resistance increased. This electrical behavior in Cycle 1 can be attributed to the initial use of DI water in the concentrate compartment. The absence of ions resulted in very low solution conductivity and high electrical resistance at the start of the cycle. As ions migrated from the diluate into the concentrate compartment, the conductivity of the concentrate increased, leading to a reduction in stack resistance and allowing higher current to pass through the system. In the later stage of the cycle, progressive ion depletion in the diluate compartment became the dominant factor, increasing the overall resistance of the ED stack and causing the observed decline in current under the voltage-limited condition.

In contrast, the electrical profiles observed in Cycles 2–18 were markedly different from those of Cycle 1 and exhibited a highly consistent and repeatable pattern. At the beginning of each of these cycles, the output current was immediately high, without the initial low-current, high-resistance phase observed in Cycle 1. The absence of the initial high-resistance phase in Cycles 2–18 can be explained by the elevated ionic conductivity already present in the concentrate compartment due to ion accumulation from previous cycles. As a result, the ED stack no longer experienced the ion-free condition characteristic of the first cycle. During each cycle, the voltage gradually increased until reaching the upper limit, after which the current decreased while the resistance continued to rise. This general pattern closely resembled the latter half of Cycle 1. The gradual increase in end-cycle current observed over successive cycles further reflects the increasing conductivity of the concentrate solution as nutrients accumulated, despite the overall rise in resistance driven by ion depletion in the diluate compartment.

The corresponding conductivity changes in the diluate and concentrate compartments are shown in Fig. 3B. Within each cycle, the conductivity of the diluate compartment decreased markedly from approximately 32–35 mS/cm to approximately 2–6 mS/cm, indicating effective removal of ions via electromigration. Simultaneously, the conductivity of the concentrate compartment increased monotonically over successive cycles, reaching a final value of approximately 190 mS/cm by the end of the experiment, demonstrating cumulative ion accumulation and successful concentration of nutrients. Notably, while the diluate conductivity exhibited a consistent cyclic depletion-recovery pattern, the concentrate conductivity followed a smooth, upward trend throughout the experiment. This behavior confirms that the fixed feed concentration strategy enabled controlled and continuous

Table 1
Ionic compositions of the MBR permeate and its distillation concentrate.

Parameter	Conductivity	TDS	Na^+	K^+	PO_4^{3-}	SO_4^{2-}	NO_3^-	NH_4^+
	(mS/cm)	(g/L)	(mg/L)	(mg/L)	(mg/L)	(mg/L)	(mg/L)	(mg/L)
MBR permeate	23.5	15.98	1190	996	144	257	1826	1907
Distillated concentrate	145	98.53	12,100	9270	1090	2470	19,947	18,966

Table 2
Physicochemical characteristics of the processed MBR permeate and its final ED concentrate obtained under acidic operations.

Parameter	Conductivity (mS/cm)	TDS (g/L)	TOC (mg/L)	Na^+ (mg/L)	K^+ (mg/L)	Mg^{2+} (mg/L)	Ca^{2+} (mg/L)	PO_4^{3-} (mg/L)	SO_4^{2-} (mg/L)	NO_3^- (mg/L)	NH_4^+ (mg/L)	Cl^- (mg/L)
Processed MBR permeate	32.8	19.9	255	3391	1957	0.023	0.015	269.5	1300	1480	1740	6812
Final ED concentrate	189.3	180	346	26,642	14,893	0.412	0.505	818	6800	11,950	12,700	51,000

enrichment of the concentrate stream without dilution. As the concentration progressed, the incremental increase in concentrate conductivity per cycle gradually diminished, suggesting increasing transport resistance and reduced marginal concentration efficiency at higher ionic strengths, consistent with prior fundamental studies [66]. This trend ultimately justified the termination of the ED process based on the marginal energy consumption criterion.

Fig. 4 summarizes the evolution of TDS, TOC, pH, and pH change in both the diluate and concentrate compartments over the 18 ED concentration cycles operated under acidic conditions. The data at Cycle 0 denote the initial solution compositions in both compartments, including the fresh feed supplied to the diluate compartment at the beginning of each cycle and the DI water present in the concentrate compartment, while the data for Cycles 1–18 represent the compositions of the diluate and concentrate solutions at the end of each ED cycle.

As shown in Fig. 4A, the TDS concentration in the concentrate compartment increased steadily with increasing cycle number and reached 180 g/L by the end of Cycle 18, corresponding to an overall concentration factor of approximately 9. In contrast, the TDS in the diluate compartment reduced from approximately 20 g/L to $\leq$3 g/L at the end of each concentration cycle throughout the experiment, indicating that most dissolved ions were effectively removed from the feed solution during each ED operation. This behavior confirms that inorganic ions were efficiently transferred from the diluate to the concentrate compartment and accumulated cumulatively in the concentrate stream over successive cycles, while no inter-cycle accumulation occurred in the diluate compartment. The near-linear increase in concentration factor during the early cycles, followed by a gradual leveling-off at later cycles, suggests diminishing concentration efficiency at higher ionic strengths, consistent with the conductivity trend. The TOC concentrations measured at the end of each cycle are presented in Fig. 4B. In the diluate compartment, the residual organic contents after an ED treatment cycle remained relatively close to those of the fresh feed, indicating that most of the organic carbon remained in the diluate compartment after each concentration cycle. In contrast, the TOC concentration in the concentrate compartment increased gradually over successive cycles, reaching approximately 346 mg/L by the final cycles. However, the corresponding TOC concentration factor was less than 1.4. This markedly lower concentration factor for TOC compared to TDS indicates that organic matter was only weakly concentrated during ED operation. This behavior reflects the limited electromigration of organic compounds, which are predominantly uncharged or weakly charged, and therefore largely retained in the diluate compartment. As a result, ED effectively concentrated inorganic ions while minimizing organic enrichment in the concentrate stream.

Fig. 4C and D shows the pH information in the diluate and concentrate compartments at the end of each cycle. The fresh feed introduced into the diluate compartment had a pH of approximately 2.3 at the start of each cycle. After each ED cycle, the pH in the diluate compartment increased to values consistently higher than the feed, ranging from 3.68 to 2.64. The magnitude of this pH increase decreased gradually with cycle number. The consistent increase in diluate pH after each cycle indicates net removal of acidity from the feed during ED operation. This behavior is consistent with preferential electromigration of H^+ from the diluate through the CEMs into the concentrate compartment under an applied electric field, thereby reducing the acidity in the diluate at the end of each cycle. The progressive decrease in ΔpH over cycles suggests that, as the concentrate solution became increasingly ion-rich and acidic, the driving forces and/or buffering conditions governing proton transport evolved, resulting in a smaller net pH rise in the treated diluate. In the concentrate compartment, the initial solution was DI water with a pH of 5.9. After Cycle 1, the concentrate pH dropped sharply to around 2.3, and then continued to decrease slowly over subsequent cycles, reaching approximately 1.35 by the end of Cycle 18. It supports the view that acidic species accumulated in the concentrate stream as ions migrated in and the concentrate composition progressively shifted away from DI water. This pH evolution is consistent with cumulative ion accumulation in the concentrate compartment under the fixed feed concentration strategy. Together, these results demonstrate that, under acidic operation, proton transport plays a dominant role in governing pH evolution in both compartments during ED concentration.

Fig. 5 presents the concentration profiles of major metal cations in the diluate and concentrate compartments during ED operation under acidic conditions. In the concentrate compartment, metal cations increased progressively over successive ED cycles. Sodium concentration rose to approximately 26 g/L by Cycle 18, corresponding to a concentration factor of approximately 7.9 relative to the feed. A similar trend was observed for potassium, with concentrate concentrations increasing steadily to approximately 15 g/L by the final cycle, achieving concentration factors on the order of 7.6.

The magnesium and calcium concentrations in the processed MBR permeate were extremely low, at approximately 0.02 mg/L. Nevertheless, their concentrations in the concentrate compartment increased gradually and continuously over successive cycles, reaching approximately 0.4 mg/L for magnesium and 0.5 mg/L for calcium by Cycle 18. In contrast, in the diluate compartment, the residual sodium and potassium concentrations after a single ED treatment decreased rapidly from their initial feed levels of approximately 3.39 g/L and 1.96 g/L to around 340–540 mg/L and 50–130 mg/L, respectively, indicating effective removal of monovalent cations during each ED operation. The magnesium and calcium concentrations in the diluate compartment after each cycle were below the detection limit and therefore are not shown.

Fig. 6 presents the concentration profiles of major nitrogen species and nutrient anions during ED concentration under acidic conditions. As shown in Fig. 6A, ammonium exhibited continuous accumulation in the concentrate compartment over successive ED cycles. The ammonium concentration increased to approximately 13 g/L by Cycle 18, corresponding to a concentration factor of approximately 7.3. In contrast, the ammonium concentration measured in the diluate compartment decreased markedly from an initial feed concentration of nearly 1.73 g/L to approximately 55–110 mg/L at the end of each cycle, indicating effective removal of ammonium during each ED operation.

Similarly, nitrate in Fig. 6B showed a clear and progressive enrichment in the concentrate compartment. The nitrate concentration increased steadily to approximately 12 g/L by the final cycle, achieving a concentration factor of 7.4. End-of-cycle nitrate concentrations in the diluate compartment remained substantially lower than in the processed MBR permeate, reducing from 1.6 g/L to approximately 30–80 mg/L, confirming efficient anion transport across the AEMs. The high concentration factors achieved for ammonium and nitrate indicate efficient electromigration of both cationic and anionic nitrogen forms, highlighting the suitability of ED for recovering total inorganic nitrogen in a concentrated liquid fertilizer.

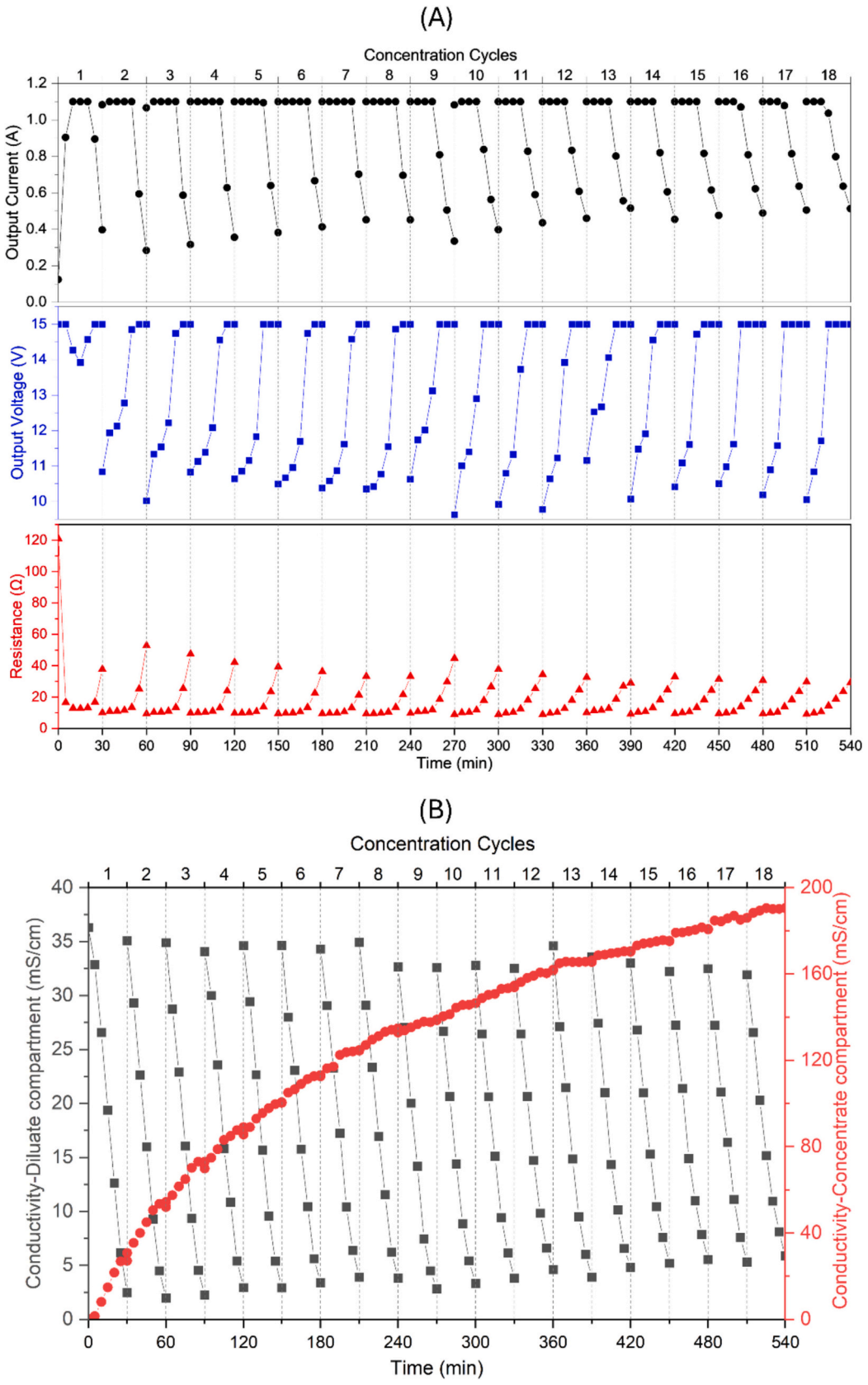

Fig. 3. Electrical response and conductivity evolution during ED concentration of processed MBR permeate under acidic conditions. (A) Output current, voltage, and calculated stack resistance during 18 consecutive concentration cycles. (B) Conductivity variation in the diluate and concentrate compartments over time.

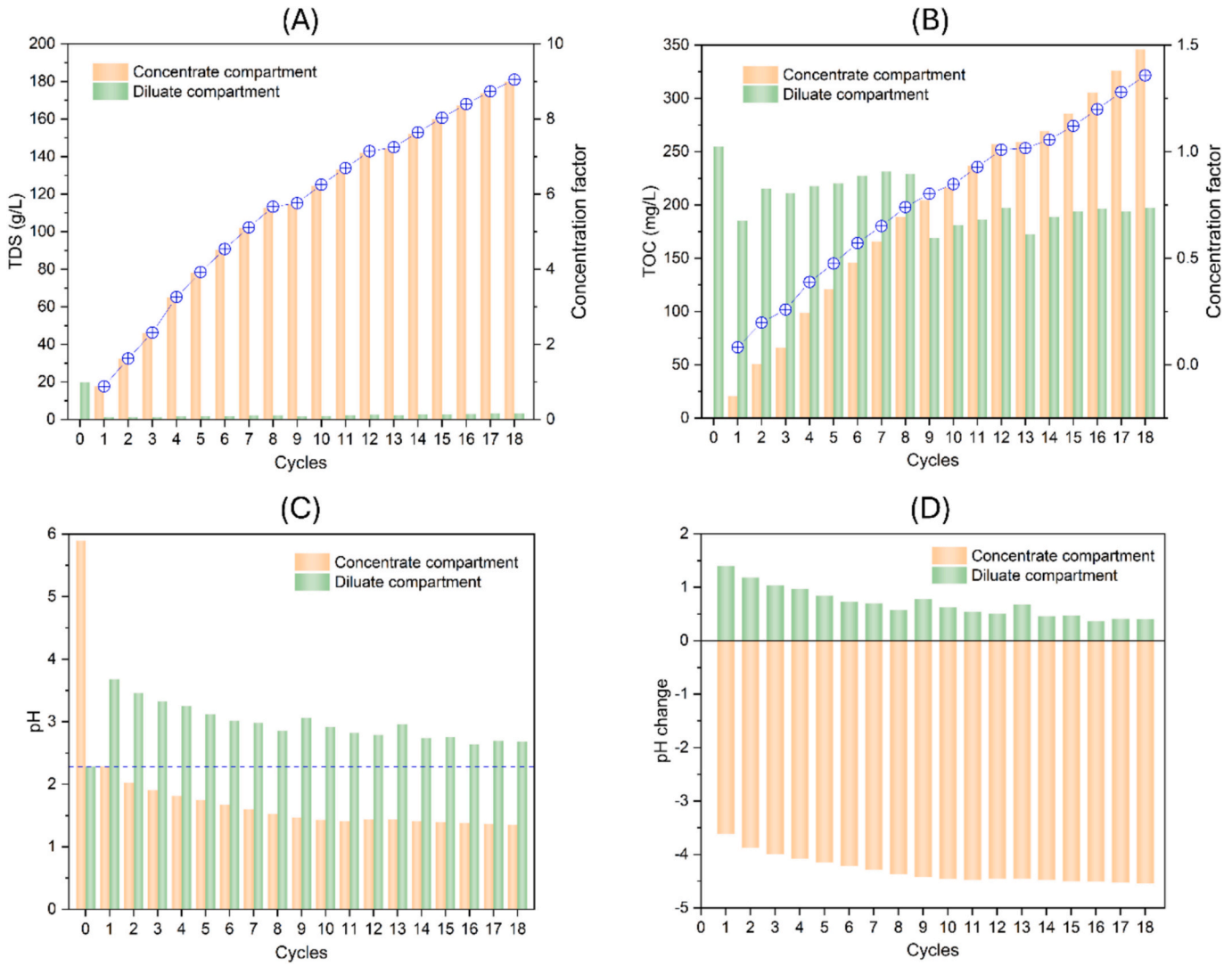

Fig. 4. Evolution of solution composition during ED concentration of processed MBR permeate under acidic conditions. (A) TDS and corresponding concentration factor, (B) TOC and concentration factor, (C) pH values, and (D) pH change relative to the initial feed in the diluate and concentrate compartments over 18 consecutive ED concentration cycles.

Phosphate accumulation in the concentrate compartment is shown in Fig. 6C. The phosphate concentration increased progressively over cycles, reaching approximately 820 mg/L by Cycle 18, corresponding to a concentration factor of approximately 3. Compared with monovalent nitrogen species, phosphate exhibited a lower concentration factor, reflecting its multivalent charge and stronger hydration. In the diluate compartment, phosphate exhibited limited removal during ED operation, decreased from an initial feed level of approximately 270 mg/L to 160–185 mg/L at the end of each cycle, corresponding to a reduction of less than half of the initial concentration. As presented in Fig. 6D, sulfate concentrations in the concentrate compartment also increased steadily over successive cycles, reaching approximately 6.8 g/L by Cycle 18, with concentration factors on the order of 5. In the diluate compartment, sulfate concentrations decreased from an initial feed level of approximately 1.34 g/L to 340–620 mg/L after each ED cycle.

The comparatively lower concentration factor observed for phosphate can be primarily attributed to its stronger electrostatic interactions with water molecules and membrane functional groups, which reduce its mobility [38,62]. Additionally, the selective enrichment patterns observed for different nutrient species also reflect the coupled effects of membrane transport mechanisms and multi-ion interactions [35,48,67–69]. Transport through ion exchange membranes can be regulated by Donnan exclusion and membrane fixed charge density, which preferentially facilitate the transport of counter-ions while limiting co-ion penetration [38,41,67,70–73]. In this multi-ion system, competitive ion transport becomes a dominant factor, as high concentrations of monovalent cations and anions occupy a large fraction of available transport pathways, effectively suppressing the flux of multivalent species [48,67,74]. This competition is further amplified by differences in diffusion coefficients and hydration shell structures, leading to preferential migration of smaller, more mobile ions [38,62,72,75–77]. Moreover, non-ideal membrane permselectivity under high ionic strength conditions may induce co-ion leakage, reducing effective separation and further limiting the enrichment of multivalent ions [38,48,67,70,71,73]. As a result, the observed transport hierarchy arises from the combined influence of ion charge, hydration properties, driving force, membrane selectivity, and membrane transport characteristics under acidic ED operation. These results further confirm that ED is capable of producing a nutrient-rich concentrate suitable for downstream fertilizer applications.

Table 2 compares the ionic compositions of the processed MBR permeate and the final ED concentrate obtained under acidic operation. Fig. 7 summarizes ion removal efficiency in the diluate compartment, ion enrichment in the concentrate compartment, and the corresponding

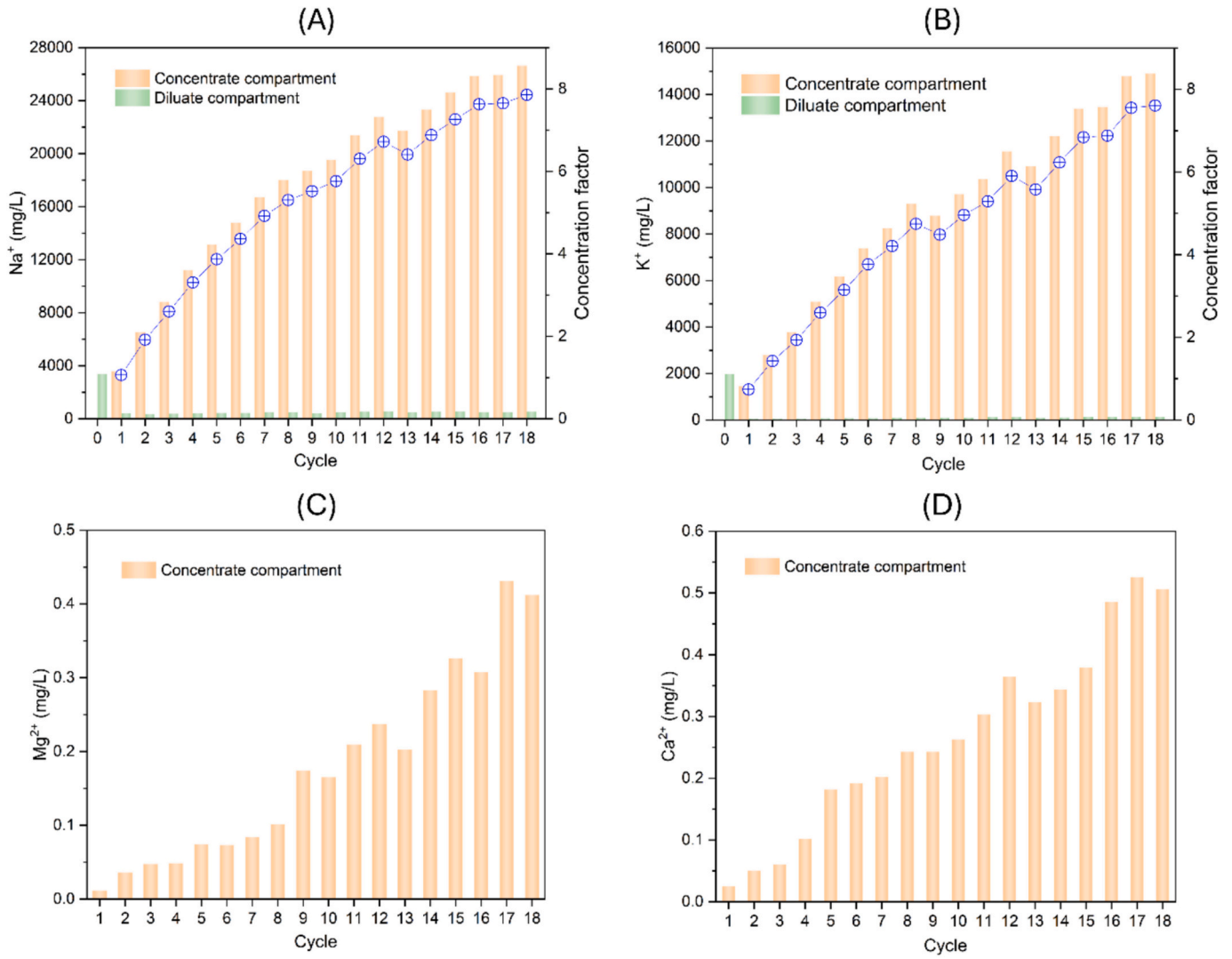

Fig. 5. Evolution of metal cation concentrations during ED concentration of processed MBR permeate under acidic conditions. (A–B) Sodium and potassium concentrations and concentration factors in the diluate and concentrate compartments, and (C–D) magnesium and calcium concentrations in the concentrate compartment over 18 consecutive ED cycles.

energy consumption during ED operation under acidic conditions. As shown in Fig. 7A, consistently high removal efficiencies were achieved for monovalent ions throughout the 18 ED cycles under acidic conditions. Sodium, potassium, ammonium, nitrate, and chloride exhibited removal efficiency generally exceeding 85% per cycle, indicating highly effective electromigration from the diluate compartment despite progressive concentration of the receiving solution. These high removal efficiencies were sustained across cycles, reflecting the strong driving force for ion transport maintained by the fixed feed concentration strategy and the high ionic mobility under acidic conditions. In contrast, multivalent anions exhibited substantially lower but stable removal efficiencies. Phosphate removal remained in the range of approximately 30–45%, while sulfate removal ranged from approximately 55–75% per cycle. Phosphate transport is further restricted due to its higher effective charge and stronger electrostatic exclusion within the AEM, resulting in a higher energetic barrier for membrane entry [21,38,62,76,78]. Moreover, under acidic conditions, phosphate exists predominantly as $H_2PO_4^-$, yet still exhibits strong interactions with membrane functional groups and surrounding hydration shells, which reduces its effective mobility [62]. In contrast, sulfate, despite being divalent, experiences relatively lower steric and electrostatic hindrance, allowing more efficient participation in competitive transport [38]. These effects, combined with competition from abundant monovalent anions, lead to the significantly suppressed transport of phosphate relative to sulfate [48,62].

The ion removal trends are directly reflected in the enrichment behavior observed in the concentrate compartment, shown in Fig. 7B. The concentration factors of monovalent ions increased steadily with ED cycles, reaching final values of approximately 7.3–7.8 by Cycle 18, demonstrating highly consistent and efficient enrichment throughout the ED operation. In contrast, phosphate exhibited a markedly lower concentration factor, increasing gradually to approximately 3.0, while sulfate reached a concentration factor of approximately 5.0. The divergent enrichment behaviors highlight the strong dependence of ED concentration performance on ion valence and mobility under acidic conditions, with monovalent species showing substantially higher concentration efficiency than multivalent ions.

The progressive enrichment of nutrients was accompanied by increasing energy demand, as shown in Fig. 7C. As the conductivity of the concentrate compartment increased to approximately 189 mS/cm, the cumulative electrical charge transfer and total energy consumption increased nonlinearly, reaching approximately 8.4 Ah and 108 Wh by the end of the operation, respectively. The close correspondence between cumulative charge and energy consumption reflects stable ED

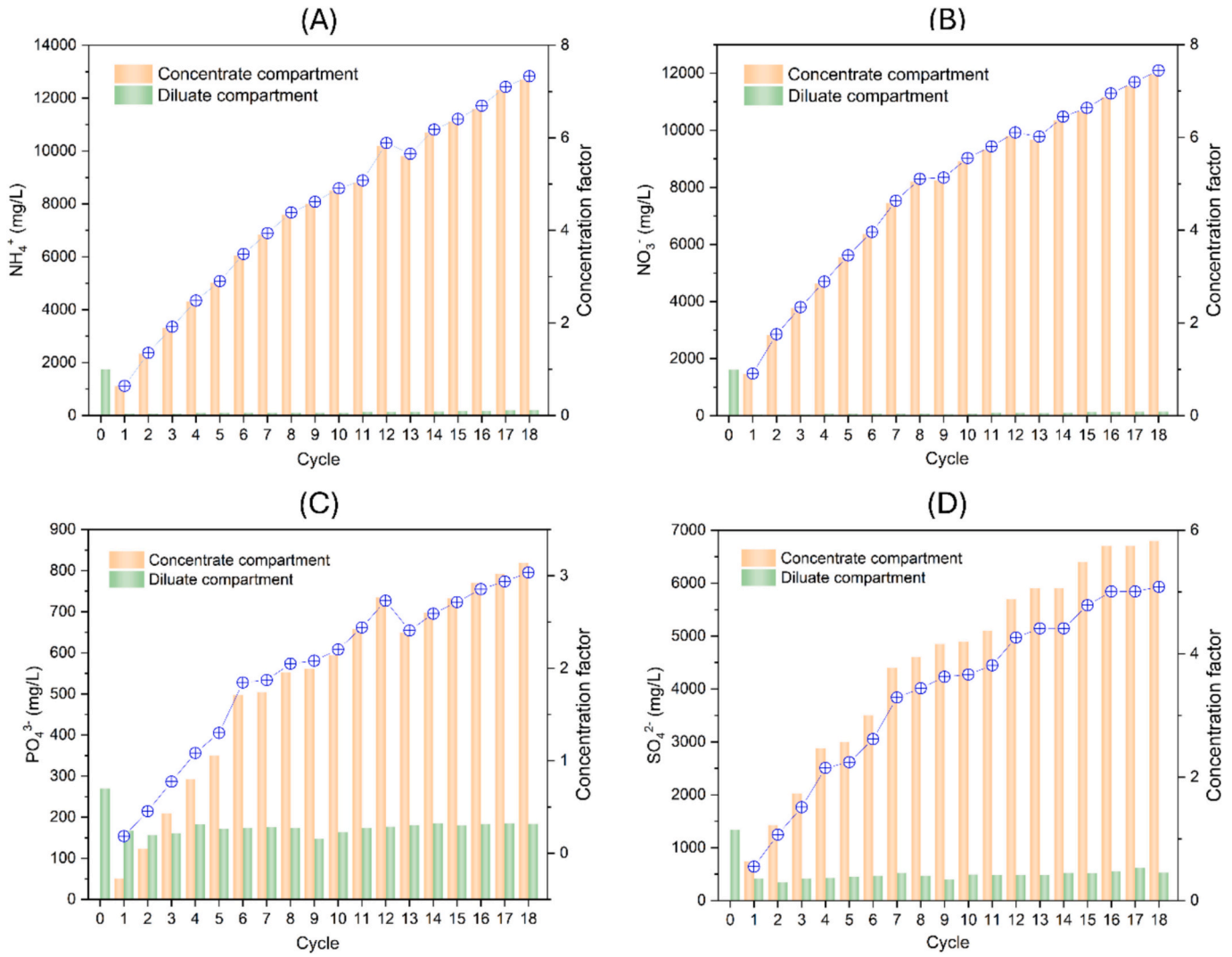

Fig. 6. Evolution of major nutrient ion concentrations during ED concentration of processed MBR permeate under acidic conditions. (A) Ammonium, (B) nitrate, (C) phosphate, and (D) sulfate concentrations and corresponding concentration factors in the diluate and concentrate compartments over 18 consecutive ED cycles.

operation, while the accelerating increase at higher conductivities indicates increased electrical resistance and polarization effects associated with highly concentrated solutions. The total apparent CE contribution from the measured ions was approximately 78%, indicating effective utilization of the applied electrical current for ion transport, with Cl^- (27.5%), Na^+ (22.2%), NH_4^+ (13.5%), and K^+ (7.3%) accounting for the largest fractions of charge transport. In contrast, multivalent ions exhibited significantly lower CE values, with SO_4^{2-} and PO_4-P contributing only 2.7% and 1.5%, respectively. This distribution indicates that a considerable fraction of the applied current was not directly associated with the net transport of the quantified species. The deviation from ideal current utilization can be attributed to several factors, including competitive ion transport among co-existing species, co-ion leakage due to non-ideal membrane permselectivity, and the contribution of unmeasured charge carriers [71]. In particular, under acidic conditions, proton (H^+) transport is expected to play a significant role due to its high mobility, thereby consuming a portion of the applied current and reducing the apparent CE of target ions. The corresponding nutrient-SEC further reflects the influence of ion transport characteristics on process efficiency, with 15.5 kWh/kg for K^+, 17.0 kWh/kg for NH_4^+, 18.1 kWh/kg for NO_3^-, and 17.2 kWh/kg for total nitrogen, indicating comparable energy requirements for monovalent ions. In contrast, significantly higher SEC values were calculated for multivalent species, particularly 264.3 kWh/kg for PO_4-P and 31.8 kWh/kg for SO_4^{2-}, highlighting the substantially greater energy demand associated with the transport of multivalent ions. This behavior is consistent with their lower current efficiency, stronger electrostatic exclusion, and intensified competition with monovalent ions, which collectively limit their transport and reduce energy efficiency.

Overall, the combined results demonstrate that ED under acidic conditions enabled efficient and selective concentration of major nutrient species, particularly monovalent ions, achieving nutrient concentration factors of up to 7–8 while maintaining moderate energy consumption. The final ED concentrate exhibited substantially increased TDS and conductivity, confirming the effectiveness of ED as an energy-efficient concentration step for producing nutrient-rich liquid fertilizer from MBR-treated urine.

During ED operation, in addition to ionic transport, a gradual water migration from the diluate compartment to the concentrate compartment was observed, with approximately 20–40 mL transferred per cycle and the magnitude increasing over successive concentration rounds. Although the diluate compartment was replenished with fresh feed at the beginning of each cycle, a clear trend emerged whereby the conductivity and ionic strength of the concentrate solution approached a quasi-plateau, while the rate of water migration continued to increase. This behavior is attributed to cumulative electro-osmotic drag, which

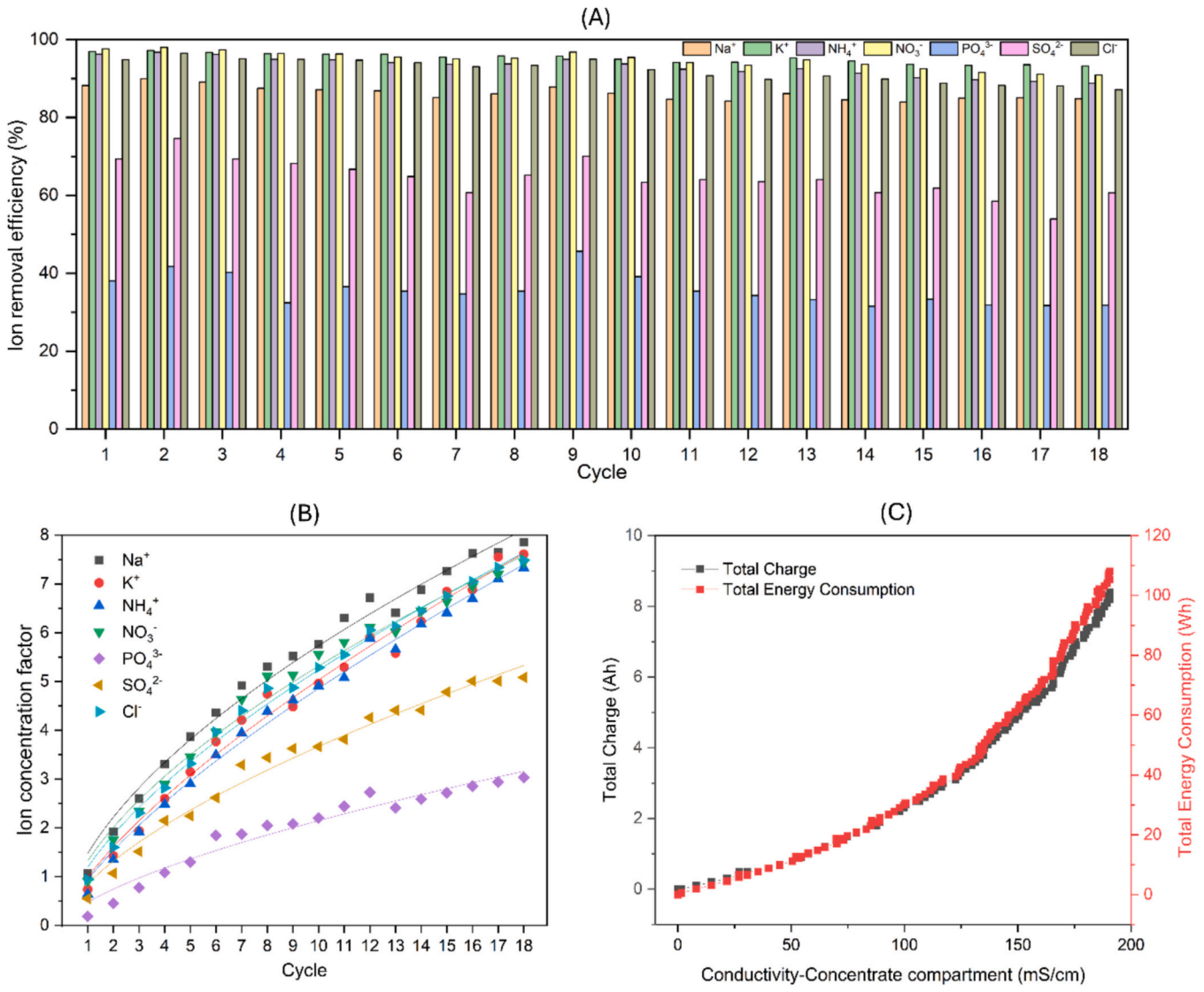

Fig. 7. Ion removal efficiency, concentration performance, and energy consumption during ED concentration under acidic conditions. (A) Cycle-resolved ion removal efficiency in the diluate compartment, (B) evolution of ion concentration factors in the concentrate compartment as a function of ED cycle number, and (C) cumulative electrical charge transfer and total energy consumption as a function of concentrate conductivity.

becomes increasingly dominant as ion concentrations in the diluate compartment decrease and the hydrated ion flux increasingly drives water transport across the membranes [79,80]. By the end of the 18th cycle, approximately 600 mL of concentrated solution was recovered in the concentrate compartment, containing a substantial fraction of the total ionic content originally present in the 9 L of processed MBR permeate treated.

3.3. ED concentration performance under near-neutral conditions

To evaluate the effect of solution pH on ED concentration behavior, the processed MBR permeate was adjusted from its original acidic condition to near-neutral pH prior to ED treatment. Specifically, the pH of the processed MBR permeate was adjusted to 6.5 using KOH, and the corresponding changes in solution composition before and after pH adjustment are summarized in Table 3. Following pH adjustment, ED concentration experiments were conducted under otherwise identical operating conditions to those used for acidic operation. Under near-neutral conditions, a total of 20 consecutive ED concentration cycles were performed using the fixed feed concentration strategy. The performance of ED under near- neutral conditions is discussed below in terms of electrical response, conductivity evolution, nutrient transport behavior, and overall concentration efficiency.

Fig. 8A presents the temporal profiles of output current, voltage, and

Table 3
Physicochemical characteristics of the processed MBR permeate before and after pH adjustment, and the final ED concentrate obtained under near-neutral operation.

Parameter	pH	Conductivity (mS/cm)	TDS (g/L)	TOC (mg/L)	Na^+ (mg/L)	K^+ (mg/L)	PO_4^{3-} (mg/L)	SO_4^{2-} (mg/L)	NO_3^- (mg/L)	NH_4^+ (mg/L)	Cl^- (mg/L)
Processed MBR permeate	2.06	37.2	22.9	321	3655	2485	291	1425	1430	2145	7700
Processed feed after pH adjustment	6.49	32.5	19.58	280	2602	2655	258	1335	1360	1890	6900
Final ED concentrate	7.32	222	179.5	534.4	29,282	28,783	681	6000	12,672	19,400	68,000

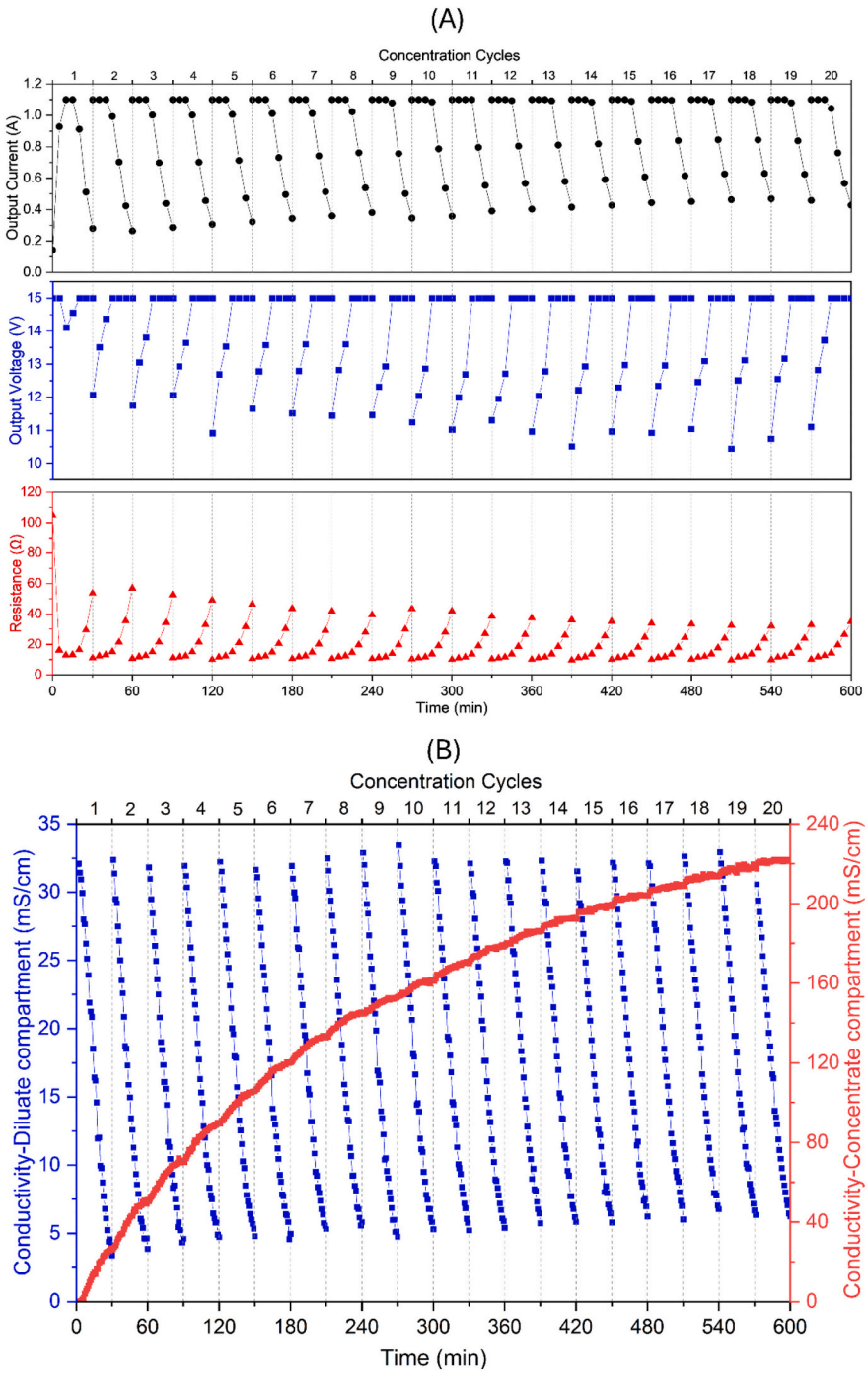

Fig. 8. Electrical response and conductivity evolution during ED concentration of processed MBR permeate under near-neutral conditions. (A) Output current, voltage, and calculated stack resistance during 20 consecutive concentration cycles. (B) Conductivity variation in the diluate and concentrate compartments over time.

calculated stack resistance of the ED system during 20 consecutive concentration cycles operated under near-neutral conditions. In Cycle 1, the concentrate compartment initially contained DI water, resulting in a high initial stack resistance, low current, and rapid attainment of the maximum voltage limit. As ions migrated from the diluate to the concentrate compartment, the concentrate conductivity increased, leading to a progressive decrease in resistance and a rise in current toward the imposed upper limit. Toward the end of Cycle 1, depletion of ions in the diluate compartment caused the resistance to increase again, accompanied by a decline in current under constant-voltage operation. From Cycle 2 onward, the electrical response exhibited a distinct and reproducible pattern that reflects stable ED operation under near-neutral conditions. At the beginning of each cycle, the current rapidly reached and remained at the preset upper limit of 1.1 A, indicating operation in constant-current mode. During this phase, the output voltage increased gradually within each cycle as resistance rose. Once the voltage reached the upper limit of 15 V, the system transitioned to constant-voltage mode, after which the current dropped sharply. The calculated resistance increased steadily during each cycle, reflecting progressive ion depletion in the diluate compartment and increasing concentration polarization effects.

Fig. 8B shows the corresponding conductivity variations in the

diluate and concentrate compartments. The feed solution introduced into the diluate compartment had an initial conductivity of approximately 32.5 mS/cm at the start of each cycle. During ED operation, the diluate conductivity decreased consistently within each cycle to values of approximately 4–6 mS/cm, indicating effective ion removal during each treatment. In contrast, the conductivity of the concentrate compartment increased cumulatively over successive cycles, rising steadily to approximately 222 mS/cm by the end of Cycle 20. Based on conductivity, this corresponds to an overall concentration factor of approximately 6.8 under near-neutral operating conditions.

Fig. 9 presents the evolution of TDS, TOC, pH, and pH change in the diluate and concentrate compartments during ED concentration under near-neutral operating conditions. TDS in the concentrate compartment increased progressively over successive ED cycles, rising from an initially negligible level to approximately 180 g/L by Cycle 20. This corresponds to an overall concentration factor of approximately 9, reflecting effective cumulative enrichment of dissolved inorganic species. In contrast, the end-of-cycle TDS values in the diluate compartment remained low, indicating efficient salt removal during each individual ED cycle.

The TOC in the concentrate compartment increased gradually from near zero to approximately 530 mg/L by the final cycle, corresponding to a concentration factor of approximately 1.9, based on the feed TOC of 280 mg/L. In contrast, TOC concentrations in the diluate compartment after each cycle remained relatively stable, generally ranging between 220 and 280 mg/L, reflecting the fact that the diluate solution was replaced with fresh feed at the beginning of each cycle. The relatively modest enrichment of TOC compared with TDS indicates that ED under near-neutral conditions preferentially concentrated inorganic ions rather than organic constituents.

The pH evolution under near-neutral ED operation differed markedly from that observed under acidic conditions. As shown in Fig. 9C, the feed solution introduced into the diluate compartment had a pH of approximately 6.5, while the concentrate compartment initially contained DI water with a pH of 5.9. After ED treatment, the pH in the concentrate compartment increased progressively over cycles, reaching approximately 7.3 by Cycle 20. In contrast, the pH in the diluate compartment decreased slightly after each cycle, with end-of-cycle values generally ranging between 5.3 and 6.1. These trends are further illustrated in Fig. 9D, which shows the pH change relative to the initial solutions in each cycle.

Unlike acidic ED operation, where pH evolution was dominated by

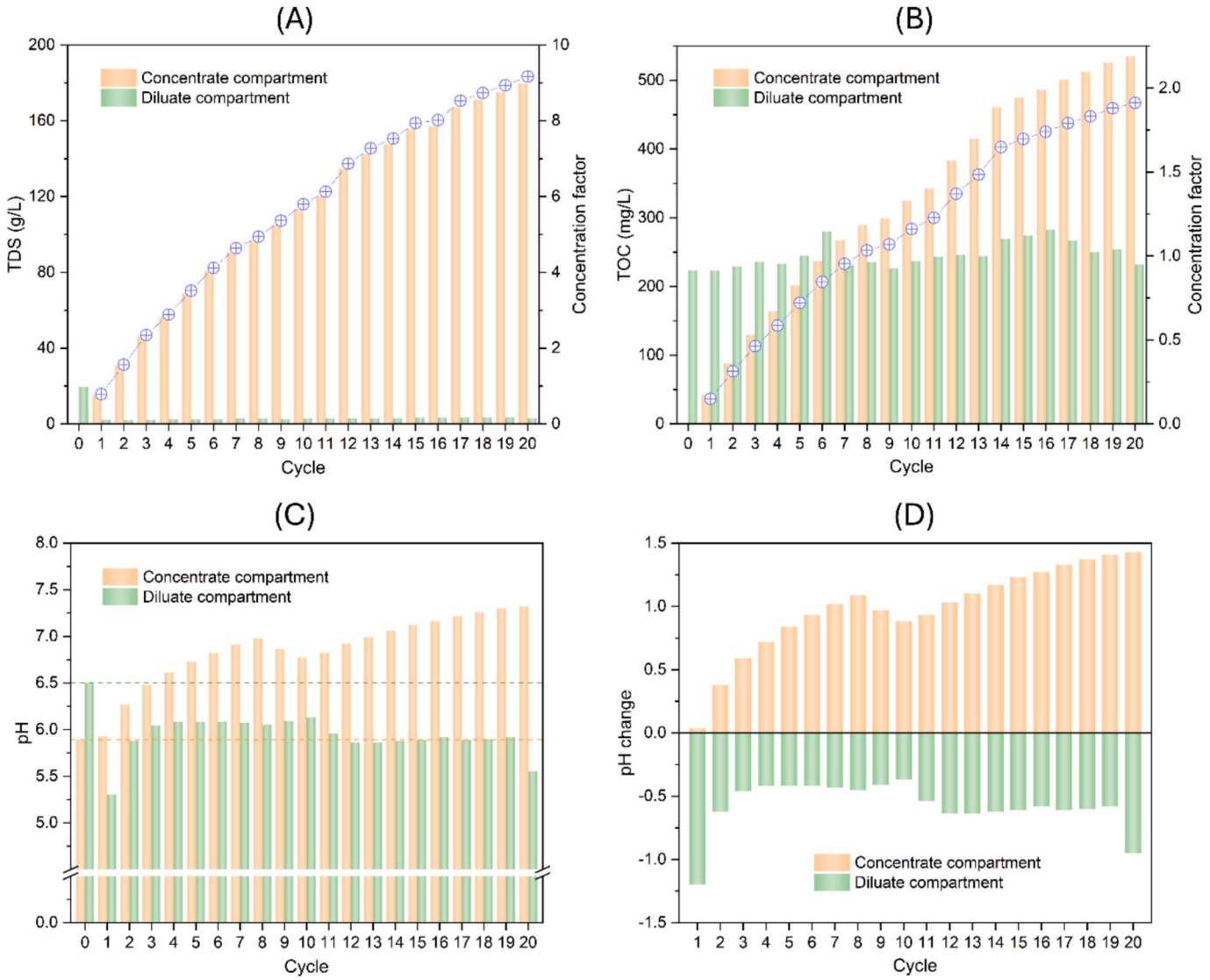

Fig. 9. Evolution of solution composition during ED concentration under near-neutral conditions. (A) TDS and corresponding concentration factor, (B) TOC and concentration factor, (C) pH values, and (D) pH change relative to the initial feed in the diluate and concentrate compartments over 20 consecutive ED concentration cycles.

direct H^+ transport and accumulation, the pH changes observed under near-neutral conditions reflect a fundamentally different governing mechanism. At near-neutral pH, the concentration of free protons in solution is low, and proton migration no longer plays a dominant role in charge transport. Instead, pH evolution is primarily governed by asymmetric ion migration, resulting local charge imbalances, and the system's compensatory response through water dissociation at membrane interfaces. At the start of ED operation, the concentrate

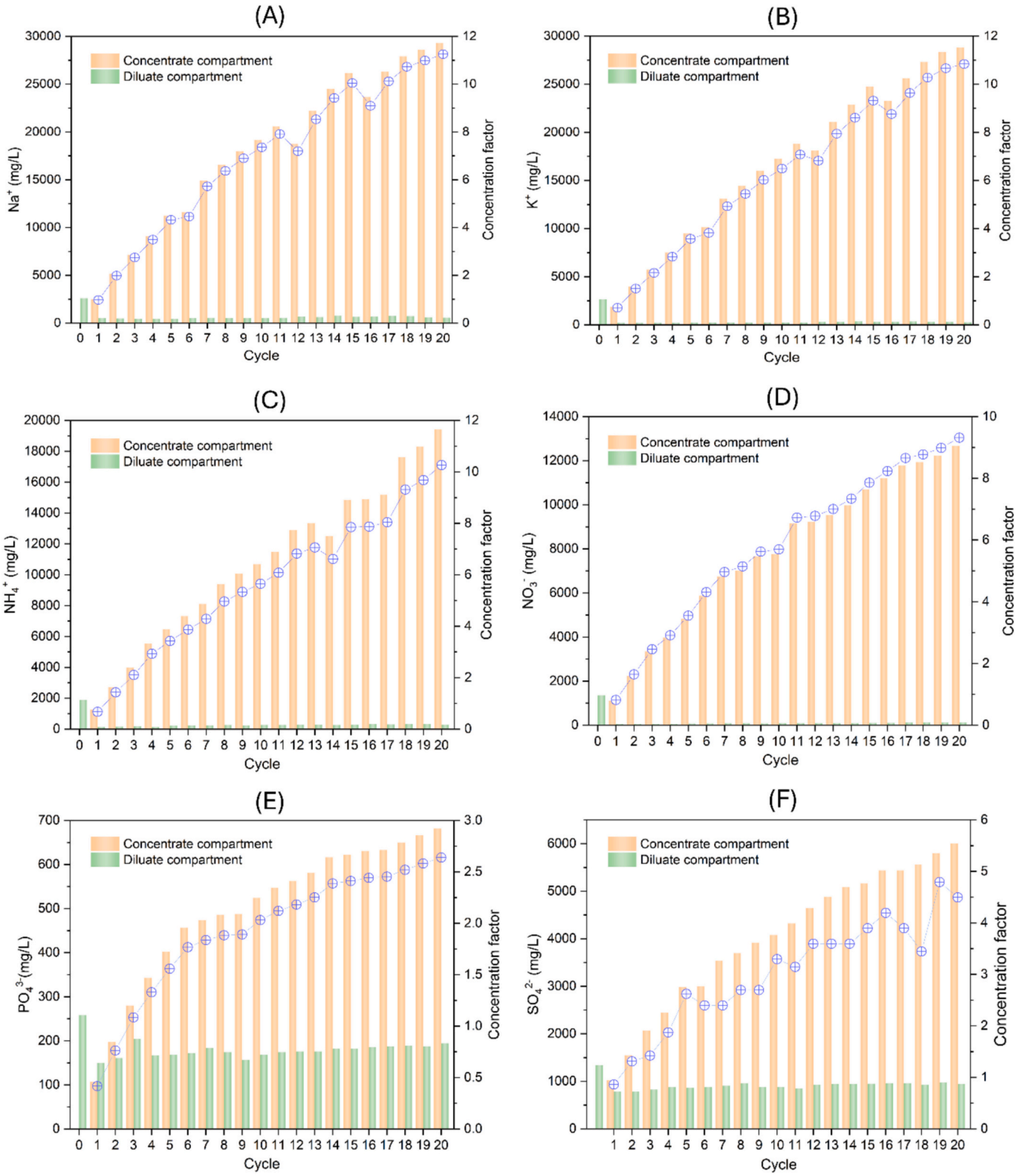

Fig. 10. Evolution of nutrient ion concentrations during ED concentration under near-neutral conditions. (A) Sodium, (B) potassium, (C) ammonium, (D) nitrate, (E) phosphate, and (F) sulfate concentrations and corresponding concentration factors in the diluate and concentrate compartments over 20 consecutive ED cycles. (Magnesium and calcium concentrations remained below detection limits and are therefore not shown.)

compartment initially contained DI water, such that the ionic composition of the concentrate was established entirely by ion migration from the feed compartment. During ED operation, differences in the transport rates of cations and anions across the ion-exchange membranes led to transient local charge imbalances. Preferential migration of cations relative to anions from the feed chamber rendered the diluate compartment relatively cation-deficient, while the concentrate compartment became relatively anion-deficient. To maintain electroneutrality, the system compensated through water dissociation, generating H^+ and OH^- ions at the membrane interfaces. In the diluate compartment, water dissociation produced H^+ to compensate for the deficit of positive charge, leading to a gradual decrease in pH. Conversely, in the concentrate compartment, water dissociation generated OH^- to balance the relative excess of positive charge, resulting in progressive alkalization. These trends were further reinforced by membrane selectivity: OH^- ions were effectively retained in the concentrate compartment due to limited back-transport across the AEMs, while H^+ ions accumulated in the diluate compartment and could not readily migrate back through the AEMs. Overall, these results demonstrate that while ED under near-neutral conditions remains effective for concentrating dissolved salts, the underlying electrochemical mechanisms governing pH evolution differ fundamentally from those under acidic operation.

Fig. 10 presents the evolution of major nutrient ion concentrations in the diluate and concentrate compartments during ED concentration under near-neutral operating conditions. As shown in Fig. 10A and B, both sodium and potassium concentrations in the concentrate compartment increased steadily over successive ED cycles to approximately 29 g/L by Cycle 20, corresponding to concentration factors of approximately 11. In contrast, the residual sodium and potassium concentrations measured in the diluate compartment at the end of each cycle were substantially lower than their respective feed concentration, consistently decreasing within each cycle from approximately 2.60 g/L to 420–800 mg/L for sodium and from approximately 2.66 g/L to 180–340 mg/L for potassium. These results indicate effective and sustained transport of monovalent cations under near-neutral ED operation.

Fig. 10C and D shows the concentration profiles of ammonium and nitrate. Both nitrogen species exhibited progressive accumulation in the concentrate compartment over successive cycles. Ammonium concentration accumulated to approximately 19.4 g/L by Cycle 20, corresponding to a concentration factor of approximately 10. Similarly, nitrate concentration increased to approximately 12.7 g/L, yielding a concentration factor of approximately 9. End-of-cycle concentrations of ammonium and nitrate in the diluate compartment remained low relative to the feed concentrations, ranging from 140 to 330 mg/L for ammonium and 50–120 mg/L for nitrate, indicating efficient electromigration of both cationic and anionic nitrogen species.

As shown in Fig. 10E and F, phosphate and sulfate exhibited distinct but consistent enrichment behaviors. Phosphate concentration in the concentrate compartment increased gradually to approximately 680 mg/L by Cycle 20, corresponding to a concentration factor of approximately 2.6. In the diluate compartment, phosphate exhibited mild per-cycle removal, with concentrations decreasing from approximately 260 mg/L in the feed to 150–200 mg/L at the end of each cycle. Compared with monovalent ions, phosphate showed more limited enrichment, consistent with its higher valence, lower mobility, and intensified membrane exclusion. Under near-neutral conditions, the reduced transport of multivalent anions becomes more pronounced. This can be attributed to a combination of enhanced electrostatic exclusion and altered speciation effects [38,62,76,78]. At higher pH, phosphate species shift toward HPO_4^{2-} and PO_4^{3-}, increasing their effective charge and strengthening Donnan exclusion within the AEM [38,62,78]. At the same time, the presence of competing monovalent ions maintains preferential occupation of transport pathways, further suppressing multivalent ion flux [48,67]. In addition, increasing ionic strength in the concentrate compartment may reduce membrane permselectivity, promoting co-ion leakage and back-diffusion, which reduces the net transport efficiency of target species [65,67,70,75,81]. Sulfate showed a more pronounced, yet still incomplete, transport behavior. Sulfate concentration in the concentrate compartment increased to approximately 6.0 g/L in the final concentrate, yielding a concentration factor of approximately 4.5. Correspondingly, sulfate concentrations in the diluate compartment decreased from an initial feed level of approximately 1.3 g/L to 780–980 mg/L after each cycle. This intermediate behavior reflects the divalent nature of sulfate and its transport characteristics relative to monovalent and trivalent species.

Table 3 compares the physicochemical characteristics of the feed solution and the final concentrate and Fig. 11 integrates ion removal efficiency in the diluate compartment, ion enrichment in the concentrate compartment, and the associated electrical energy consumption during ED operation under near-neutral operations. As shown in Fig. 11A, high and stable removal efficiencies were achieved for monovalent ions throughout the 20 ED cycles. Sodium, potassium, ammonium, nitrate, and chloride consistently exhibited removal efficiency of approximately 80–95% per cycle, indicating effective electromigration from the diluate compartment despite the progressive increase in concentrate salinity. This sustained removal performance confirms that refreshing the diluate compartment with fresh feed at the start of each cycle maintained a strong driving force for ion transport, even at elevated stack resistance in later cycles. In contrast, multivalent anions displayed notably lower removal efficiencies. Phosphate and sulfate removal ranged from approximately 20–40%, reflecting their reduced transport rates through AEMs, consistent with the previous observed patterns, due to higher valence, enhanced electrostatic exclusion, altered speciation effects, and co-ion leakage and back-diffusion [71,75,81]. The relatively stable yet lower removal efficiency for phosphate and sulfate across cycles indicate that their transport was not limited by concentration polarization but rather by intrinsic membrane selectivity and ion mobility. The ion enrichment behaviors in the concentrate compartment align closely with their cycle-wise removal efficiencies observed in the diluate compartment. As shown in Fig. 11B, monovalent ions showed near-linear increases in concentration factor with cycle number, while phosphate and sulfate exhibited more moderate enrichment trends.

Fig. 11C shows that both cumulative electrical charge transfer and total energy consumption increased nonlinearly with rising concentrate conductivity. As the concentrate conductivity increased to approximately 222 mS/cm, the cumulative charge reached 8.8 Ah, while total energy consumption increased to approximately 122 Wh. The divergence between charge and energy curves at higher conductivities indicates increasing voltage demand associated with elevated ionic strength and concentration polarization. Nevertheless, the sustained ion removal efficiencies and monotonic enrichment trends demonstrate that ED under near-neutral conditions remains effective for nutrient concentration, even at advanced concentration stages. The total apparent CE for the 20-cycle operation was estimated to be approximately 82.2%, indicating that the majority of the applied current was accounted for by the transport of quantified ionic species. Among these, Cl^- (29.2%), Na^+ (19.4%), NH_4^+ (16.4%), K^+ (11.3%) dominated current utilization, while multivalent ions showed minimal contributions, with SO_4^{2-} (1.9%) and PO_4-P (1.0%) remaining significantly suppressed. Compared with acidic operation, the slightly higher overall current utilization suggests reduced contributions from unmeasured charge carriers such as protons, consistent with the absence of strong proton-driven transport under near-neutral conditions. Nevertheless, the total CE remains below unity, indicating that a portion of the applied current is still consumed by secondary processes, including co-ion leakage, back diffusion, transport of unquantified species, and minor contributions from H^+/OH^- [71]. The corresponding energy consumption further reflects these transport characteristics, with comparable SEC values observed for monovalent ions (8.5–19.3 kWh/kg for K^+, NH_4^+, and NO_3^-), while PO_4-P exhibited a substantially higher SEC (358.9 kWh/kg), highlighting the strong energetic penalty associated with multivalent ion transport.

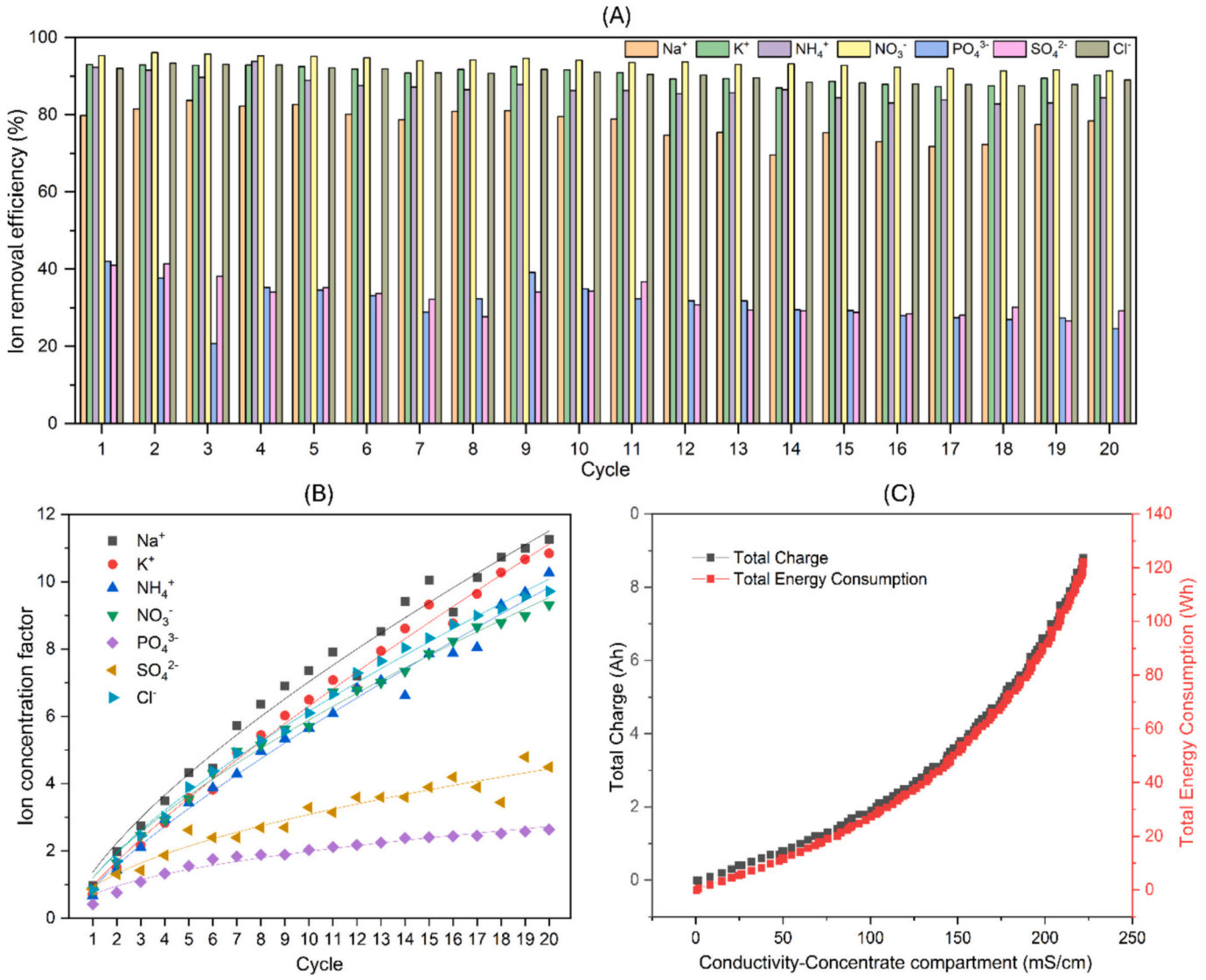

Fig. 11. Ion removal efficiency, concentration performance, and energy consumption during ED concentration under near-neutral conditions. (A) Cycle-resolved ion removal efficiency in the diluate compartment, (B) evolution of ion concentration factors in the concentrate compartment as a function of ED cycle number, and (C) cumulative electrical charge transfer and total energy consumption as a function of concentrate conductivity.

These results confirm that current distribution and energy efficiency in the system are governed by competitive multi-ion transport and membrane selectivity effects.

3.4. *Comparative evaluation of ED performance under acidic and near-neutral operating conditions*

Table 4 provides a quantitative comparison of ED performance under acidic and near-neutral operating conditions in terms of final concentration factors and cycle-resolved ion removal efficiencies. Although both operating modes enabled effective nutrient concentration, distinct differences were observed in enrichment behavior, removal efficiency, and selectivity among different ionic species, highlighting the critical role of solution pH in governing ED transport mechanisms.

To achieve comparable final TDS levels, near-neutral ED operation attained a higher conductivity-based concentration factor than acidic operation, primarily driven by enhanced enrichment of monovalent nutrient ions. Accordingly, near-neutral conditions consistently outperformed acidic conditions in terms of final concentration factors for major monovalent species. However, this higher enrichment was accompanied by lower removal efficiency in the diluate compartment under near-neutral conditions, particularly for sodium and potassium. For example, sodium removal decreased from 84.0 to 90.0% under acidic conditions to 69.6–83.7% under near-neutral conditions, while potassium removal declined from 93.2–97.2% to 87.0–93.0%. This

Table 4
Comparative performance of ED under acidic and near-neutral operating conditions in terms of final concentration factors and cycle-resolved ion removal efficiencies.

Parameter	Final concentration factor		Removal Efficiency (%)	
	Acidic	Near neutral	Acidic	Near neutral
Conductivity	5.77	6.83	82.1–93.3	80.5–88.1
TDS	9.05	9.17	84.2–94.3	82.7–89.8
TOC	1.36	1.91	9.2–33.8	9.2–20.2
Na^+	7.86	11.25	84.0–90.0	69.6–83.7
K^+	7.61	10.84	93.2–97.2	87.0–93.0
PO_4^{3-}	3.04	2.64	31.5–45.6	20.7–42.1
SO_4^{2-}	5.08	4.49	53.9–74.6	26.6–41.4
NO_3^-	7.45	9.32	90.9–98.0	91.4–96.1
NH_4^+	7.33	10.26	88.8–96.8	82.8–93.8
Cl^-	7.49	9.86	87.2–96.5	87.5–93.3

trade-off suggests that acidic conditions promote faster, more complete single-cycle ion extraction, whereas near-neutral conditions favour long-term accumulation in the concentrate compartment. This difference can be attributed to the dominant role of proton transport under acidic conditions [78]. The high mobility of H^+ enhances current efficiency and short-term ion removal but also competes with other cations for transport through the CEMs, limiting their ultimate concentration in the concentrate compartment. Under near-neutral conditions, the reduced influence of H^+ allows monovalent nutrient ions to carry a larger fraction of the electrical current, resulting in higher concentration factors despite slightly lower per-cycle removal efficiencies [78].

The distinct behaviors observed for phosphate and sulfate demonstrate that ED performance in complex waste streams is governed by a coupled mechanism and highlight the interplay between ion properties, membrane selectivity, and solution chemistry [34,38,48]. Phosphate exhibited consistently low concentration factors under both conditions, reaching 3.04 under acidic and 2.64 under near-neutral operation. Removal efficiencies were also limited, particularly under near-neutral conditions. Sulfate showed intermediate behavior between monovalent and trivalent species. Acidic operation resulted in both higher concentration factor and substantially higher removal efficiency compared with near-neutral conditions. While higher valence inherently reduces ion mobility, the extent of transport limitation is strongly modulated by pH-dependent speciation, membrane charge interactions, and competitive transport dynamics [38,62,67,74,78]. Under acidic conditions, partial protonation of phosphate reduces its effective charge, thereby weakening electrostatic exclusion and slightly enhancing its transport [81,82]. In contrast, under near-neutral conditions, the dominance of more highly charged phosphate species significantly increases Donnan exclusion and suppresses membrane permeation [62,78,82]. Moreover, the gradual increase in concentrate pH during near-neutral ED further favours the formation of multivalent phosphate species, potentially limiting phosphate transport in later cycles [65]. Furthermore, the presence of abundant monovalent ions imposes a competitive transport environment, in which ions with higher mobility and lower charge preferentially migrate, effectively limiting the flux of multivalent species [48,67]. This competition, combined with potential co-ion leakage under high ionic strength conditions, leads to reduced effective separation and contributes to the observed differences between operating conditions [65,67,70,71,81].

TOC exhibited the lowest concentration factors among all measured components, with values of 1.36 under acidic and 1.91 under near-neutral conditions, and consistently low removal efficiency. This confirms that ED primarily concentrates inorganic ions, while organic matter is largely retained in the diluate compartment. The slightly higher TOC concentration under near-neutral conditions may reflect enhanced electro-osmotic drag or weak association between organic species and migrating ions, but overall TOC transport remained limited under both operating modes.

Fig. 12 provides a direct comparison of energy consumption as a function of concentration performance under acidic and near-neutral ED operation. For a given conductivity level, acidic operation generally required slightly higher cumulative energy input than near-neutral operation, particularly at intermediate-to-high concentration levels. This indicates that near-neutral ED operation utilizes electrical energy more efficiently for sustained ionic accumulation once initial concentration thresholds are exceeded. Similarly, for monovalent cations, higher energy consumption was required to reach comparable concentrations under acidic conditions, consistent with competitive current carriage by highly mobile protons. Potassium exhibited the most pronounced divergence between the two operating modes. In contrast, phosphate displayed a different energy-concentration relationship. Although acidic operation required marginally lower energy input to achieve a given phosphate concentration, the attainable phosphate concentration range remained limited. Under near-neutral conditions, energy consumption increased more sharply at higher phosphate concentrations, reflecting increased transport resistance associated with the formation of divalent phosphate species and stronger electrostatic exclusion at elevated pH. This observation is consistent with the pH-dependent phosphate speciation effects discussed earlier and underscores the intrinsic limitations of ED for concentrating multivalent anions.

Overall, the comparative results reveal a clear trade-off between acidic and near-neutral ED operation. Acidic conditions favour high per-cycle ion removal efficiency and enhanced transport of divalent anions, providing a modest energetic advantage for multivalent species. In contrast, near-neutral conditions enable substantially higher final concentration factors and superior energy efficiency for monovalent nutrient ions, which dominate the agronomic value of urine-derived fertilizers. These findings highlight pH control as a key operational parameter for optimizing ED-based nutrient recovery systems.

3.5. Energy efficiency comparison between ED- and distillation-based concentration processes

To contextualize the energy performance of ED for nutrient concentration, a direct comparison with conventional distillation-based concentration was conducted. Thermal distillation is widely used for concentrating nutrient-rich streams; however, these processes are inherently energy-intensive due to the need to vaporize large volumes of water. In addition, prolonged thermal exposure may induce nutrient loss, ammonia volatilization, or degradation of heat-sensitive components. Such drawbacks limit the applicability of distillation for decentralized sanitation and resource recovery systems, where compact design, low energy demand, and operational simplicity are critical. In contrast, ED enables selective ion transport without phase change, offering the potential for substantially improved energy efficiency and nutrient preservation. To quantitatively compare the energy efficiency of ED and thermal distillation for nutrient concentration, the specific energy consumption normalized to individual nutrients (SEC@nutrient, kWh/kg nutrient) was employed as a unified performance metric. This normalization accounts for both concentration level and recovers nutrient mass, enabling a fair comparison between fundamentally different concentration mechanisms. Table 5 summarizes the SEC@nutrient values for potassium, ammonium, nitrate, phosphate, and sulfate achieved by distillation and ED.

For monovalent nutrient species, ED exhibited orders-of-magnitude lower energy consumption than thermal distillation. The SEC@potassium decreased dramatically from approximately 626 kWh/kg-K^+ for distillation to 8.5 kWh/kg-K^+ for ED under near-neutral pH condition, corresponding to an energy reduction of nearly two orders of magnitude. Similar trends were observed for nitrogen species, with 301 kWh/kg-N by distillation but 13.6–17.2 kWh/kg-N by ED. SEC@ammonium and SEC@nitrate were reduced approximately 94–96% and 93–94%, respectively, from thermal distillation to ED. For phosphate and sulfate, ED saved 93–95% and 98–99% SEC, respectively, compared with distillation, although the absolute energy demand remained significantly higher than for monovalent nutrients. The energy efficiency of ED compared with distillation demonstrates that electrically driven separation remains more favorable than distillation, even for challenging multivalent species.

3.6. Performance comparison with reported ED-based nutrient recovery systems

To further contextualize the performance of this ED system, a comparative analysis was conducted against representative ED studies reported in the literature, covering a range of feed types including urine, anaerobic digestate, and synthetic wastewater, as listed in Table 6. The comparison focuses on key performance indicators including final nutrient concentration, concentration factor, removal efficiency, energy consumption, and current efficiency.

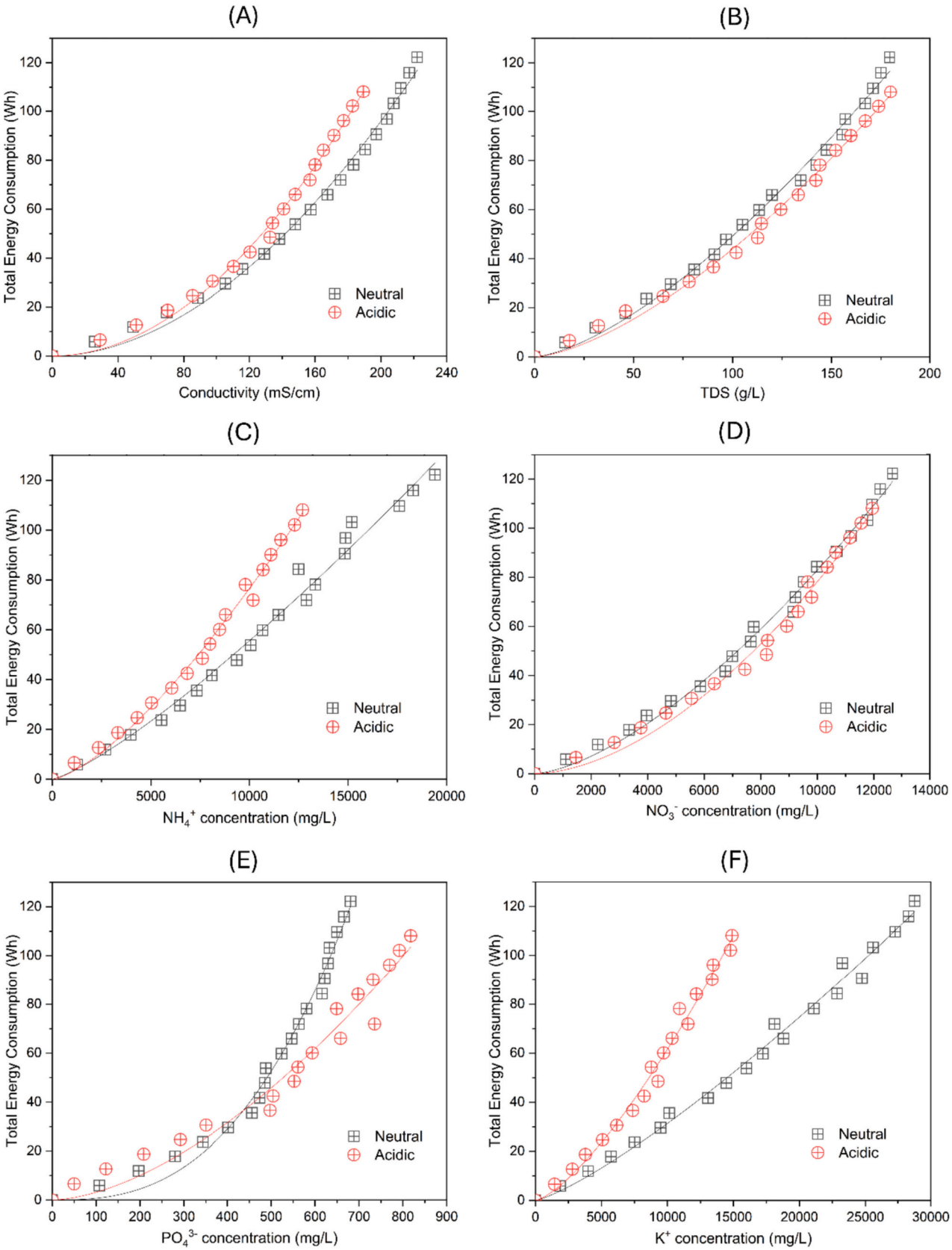

Fig. 12. Comparison of cumulative energy consumption during ED under acidic and near-neutral operating conditions as a function of concentration performance: (A) conductivity, (B) TDS, (C) ammonium, (D) nitrate, (E) phosphate, and (F) potassium.

Table 5
Comparison of normalized specific energy consumption (SEC@ nutrient) for nutrient concentration using thermal distillation and ED.

SEC@nutrient (kWh/kg-nutrient)	Distillation	ED (acidic pH)	ED (near-neutral pH)
SEC@potassium (kWh/kg-K^+)	626	15.5	8.5
SEC@ammonium (kWh/kg-NH_4^+)	306	17.0	12.6
SEC@nitrate (kWh/kg-NO_3^-)	291	18.1	19.3
SEC@nitrogen (kWh/kg-N)	301	17.2	13.6
SEC@phosphate (kWh/kg-PO_4-P)	5321	264.3	358.9
SEC@sulfate (kWh/kg-SO_4^{2-})	2348	31.8	40.7

A cross-comparison of the reported studies reveals that ED performance is primarily governed by the interplay between feed composition, system configuration, and ion transport competition. Systems treating simplified or pre-conditioned feeds tend to achieve higher apparent efficiencies or concentration levels, whereas performance declines in complex, multi-ion matrices due to competitive transport and non-ideal membrane selectivity. This is particularly evident in the consistently lower recovery and enrichment of multivalent species such as phosphate across all studies. Another key trend is the trade-off between concentration performance and process complexity. While staged or hybrid ED configurations can significantly enhance concentration factors and final product concentrations, these improvements are typically accompanied by increased energy demand and operational complexity. In contrast, simpler operations often exhibit limited enrichment capability.

Within this context, this study demonstrates a balanced performance profile, achieving relatively high concentration factors and product concentrations for monovalent nutrients under a single-stage configuration. This suggests that the integration of MBR pretreatment effectively conditions the feed solution, enabling improved ion transport without the need for additional staging or advanced system modifications. Importantly, the system maintains high removal efficiency for monovalent ions including NH_4^+, NO_3^-, K+, while exhibiting the expected limitations for multivalent species, consistent with fundamental ED transport mechanisms. The observed energy consumption falls within the range reported for complex wastewater systems, indicating that the improved concentration performance is not achieved at the expense of disproportionate energy input. Overall, the comparison highlights that the proposed system achieves a favorable balance between process efficiency and operational simplicity under realistic multi-ion conditions, which is critical for practical implementation in decentralized nutrient recovery.

4. Conclusions

This study systematically demonstrated an integrated MBR-ED system as an efficient and energy-saving approach for nutrient recovery from source-separated human urine. The results demonstrate that the integration of biological stabilization with electrochemical concentration provides a synergistic pathway for decentralized urine valorization, where MBR ensures process stability and product safety, and ED enables efficient nutrient concentration. By coupling biological stabilization with electrically driven ion concentration, the proposed process enables selective enrichment of fertilizer-relevant nutrients while avoiding the high energy demand and thermal drawbacks associated with conventional concentration methods. The MBR effectively stabilized

Table 6
Comparison of ED performance metrics for nutrient recovery.

Feed type	System configuration	Target nutrients	Final nutrient concentration	Concentration factor	Removal efficiency	Energy consumption	Current efficiency	Ref.
Diluted, pretreated urine	Precipitation + nitrification + ED	NO_3^-, PO_4-P, K^+	NO_3^-: 5.1 g/L; PO_4-P: 120 mg/L; K^+: 2.3 g/L	NO_3^-: 4.3; PO_4^{3-}: 2.6; K^+: 4.6	NO_3^-: 70%; PO_4^{3-}: 38%; K^+: 83%	N/A	N/A	[45]
Anaerobic digester centrate	Pilot-scale ED	NH_4^+, K^+	NH_4^+: 7.1 g/L; K^+: 2.49 g/L	NH_4^+: 8.77	NH_4^+: 40%; K^+: 14%	4.9 ± 1.5 kWh/kg-N	76 ± 2%	[49]
Hydrolyzed urine	ED	NH_4^+, PO_4-P, K^+	NH_4^+: 30.1 g/L; PO_4-P: 0.58 g/L; K^+: 11.5 g/L	NH_4^+: 3.5; PO_4-P: 4.1; K^+:3.4	NH_4^+: 64%	9.0 ± 0.2 kWh/kg-N	70%	[1]
Synthetic urine	3-Chamber electro-concentration	NH_4^+	NH_4^+: 36.1–88.4 g/L	N/A	NH_4^+: 43–57%	N/A	N/A	[67]
Industrial anaerobic effluent	SED	PO_4^3-P	PO_4-P: 0.855 g/L	6.5	N/A	16.7 kWh/kg-P	72%	[62]
Anaerobic swine digestate	ED	NH_4^+	N/A	N/A	70.8–99.1%	0.24–15.2 kWh/kg-N	55.1–85.5%	[83]
Synthetic wastewater	ED	NH_4^+, PO_4-P	NH_4^+: 753–838 mg/L; PO_4-P: 39.9–58.4 mg/L; K^+: 291–307 mg/L; SO_4^{2-}: 64–149 mg/L	N/A	NH_4^+: 56–63%; PO_4-P: 87–90%; K^+: 33–38%; SO_4^{2-}: 76–77%	1.01 kWh/kg N; 89.7 kWh/kg-P; 5.22 kWh/kg-K	37.4–45.4%	[48]
Municipal wastewater	Single-/two-stage ED	NO_3^-	NO_3^-: Single-stage 0.46 g/L; two-stage 1.92 g/L	Single-stage: 4.6; two-stage: 19.2	N/A	Single-stage: 6.37 kWh/kg NO_3^-; two-stage: 19.2 kWh/kg NO_3^-	N/A	[56]
Simulated wastewater	Hardness removal + staged ED	NH_4^+	NH_4^+: 5.7 g/L (single stage), 25.3 g/L (staged)	Single stage: 9–13; three-stage: 49.5	N/A	Single-stage: 15.18 kWh/kg-N; three-stage: 17.25 kWh/kg-N	N/A	[84]
Source-separated human urine	MBR + ED	NH_4^+, NO_3^-, PO_4^{3-}P, K^+, SO_4^{2-}	NH_4^+: 12.7–19.4 g/L; NO_3^-: 12.0–12.7 g/L; PO_4^{3-}P: 0.68–0.82 g/L; K^+: 14.9–28.8 g/L; SO_4^{2-}: 6.0–6.8 g/L	NH_4^+: 7.3–10.3; NO_3^-: 7.4–9.3; PO_4^{3-}P: 2.6–3.0; K^+: 7.6–10.8; SO_4^{2-}: 4.5–5.1	NH_4^+: 89–96%; NO_3^-: 91–98%; PO_4^{3-}P: 32–46%; K^+: 93–97%; SO_4^{2-}: 54–75%	13.6–17.2 kWh/kg-N; 8.5–15.5 kWh/kg-K	78–82%	This work

N/A: not reported in the literature.

hydrolyzed urine and produced a permeate with a stable ionic matrix suitable for downstream ED treatment. Subsequent ED operation successfully concentrated major inorganic nutrients under both acidic and near-neutral conditions through a fixed feed concentration strategy. Comparative analysis revealed a clear trade-off between acidic and near-neutral ED operation. Near-neutral conditions enabled substantially higher final concentration factors and superior energy efficiency for monovalent nutrient ions, which dominate the agronomic value of urine-derived fertilizers. The observed differences were attributed to pH-dependent ion speciation, proton competition, and membrane transport mechanisms, highlighting pH control as a critical operational lever for optimizing ED performance. The energy efficiency comparison between ED and thermal distillation further underscored the advantages of electrically driven concentration. When evaluated using nutrient-normalized specific energy consumption (SEC@nutrient), ED reduced energy demand by one to two orders of magnitude compared with distillation. These findings demonstrate that ED decouples nutrient concentration from bulk water removal, enabling targeted, low-energy recovery of valuable nutrients.

Despite the promising performance of the MBR-ED system, some limitations remain. Sodium was co-concentrated during ED operation, which may negatively affect fertilizer quality at high application rates, highlighting the need for strategies enabling selective sodium removal. In addition, phosphorus recovery was comparatively limited due to its multivalent nature and pH-dependent speciation, suggesting that pH-tailored operation or hybrid separation approaches may be required to further enhance phosphorus recovery. Overall, the integrated MBR-ED system provides a technically simple, energy-efficient, and modular strategy for valorising human urine as a nutrient resource. The insights gained into pH-dependent transport behavior and nutrient-specific energy efficiency offer important guidance for process design and optimization. This work highlights the strong potential of membrane-based hybrid systems for decentralized sanitation, circular nutrient management, and sustainable fertilizer production.

Declaration of competing interest

The authors declare no conflict of interest. Ho Kyong Shon serves as a co-Editor-in-Chief in the Desalination journal, whereas the editorial and peer-review processes of this manuscript were administered by another Editor.

Acknowledgements

The Australian Research Council (ARC) industrial transformation research hub on nutrients in a circular economy (NiCE) (IH210100001) supported this research.

Appendix A. Supplementary data

Supplementary data to this article can be found online at https://doi.org/10.1016/j.desal.2026.120291.

Data availability

Data will be made available on request.

References

[1] Y. Zhang, V. Koskue, G.Q. Chen, S.E. Kentish, S. Freguia, Nutrient recovery from hydrolysed urine by high-rate electrodialysis: a proof-of-concept study, Desalination 621 (119733) (2026).
[2] M.A. Barton, D. Alrousan, L.F. Perez-Mercado, S.S. Dalahmeh, A. Vasiljev, J.-O. Drangert, P. Simha, Clean enough? Acceptance of urine-derived dry fertilizer and water shaped by religious and social norms in a water-scarce Islamic context, Desalination 623 (119804) (2026).
[3] W. Sohn, A. Merenda, A.H. Shafaghat, S. Phuntsho, L. Gao, H.K. Shon, Pilot-scale membrane bioreactor for source-separated urine: impact of hydraulic retention time on fertiliser production, Desalination 616 (119388) (2025).
[4] W. Sohn, J. Jiang, S. Phuntsho, Y. Choden, V.H. Tran, H.K. Shon, Nutrients in a circular economy: role of urine separation and treatment, Desalination 560 (116663) (2023).
[5] Y. Gao, B. Vinneras, P. Simha, Partitioning behavior and crystallization of urea, salts and water during stepwise dehydration of acidified human urine by evaporation, Sci. Total Environ. 966 (178709) (2025).
[6] X. Lin, Z. Jin, S. Jiang, Z. Wang, S. Wu, K. Bei, M. Zhao, X. Zheng, Fertilizer recovery from source-separated urine by evaporation with a combined process of dehumidification and the addition of absorbent resin supplement, Water Res. 248 (120865) (2024).
[7] K.R. Karande, F. Lipnizki, B. Wu, Electrodialysis with sacrificial magnesium anode for nutrient recovery from primary municipal wastewater: effect on membrane fouling behaviours, Desalination 592 (118150) (2024).
[8] H. Chen, U. Shashvatt, F. Amurrio, K. Stewart, L. Blaney, Sustainable nutrient recovery from synthetic urine by Donnan dialysis with tubular ion-exchange membranes, Chem. Eng. J. 460 (141625) (2023).
[9] Y. Lyu, X. Ao, S. Cheng, N. Liu, Y. Men, Z. Li, Simultaneous recovery of nutrients and water from human urine by a novel thermally activated peroxydisulfate and membrane distillation integrated system, Chem. Eng. J. 459 (141548) (2023).
[10] Y. Li, R. Wang, S. Shi, H. Cao, N.Y. Yip, S. Lin, Bipolar membrane electrodialysis for ammonia recovery from synthetic urine: experiments, modeling, and performance analysis, Environ. Sci. Technol. 55 (21) (2021) 14886–14896.
[11] A. Soo, L. Gao, H.K. Shon, Roadmap for Australian wastewater nutrient recovery – towards a sustainable circular economy, Desalin. Water Treat. 323 (101273) (2025).
[12] U. Badeti, J. Jiang, S. Kumarasingham, A. Almuntashiri, N.K. Pathak, A. Chanan, S. Freguia, W.L. Ang, N. Ghaffour, H.K. Shon, S. Phuntsho, Source separation of urine and treatment: impact on energy consumption, greenhouse gas emissions, and decentralised wastewater treatment process, Desalination 583 (2024) 117633.
[13] J. Jiang, P. Dorji, U. Badeti, W. Sohn, S. Freguia, S. Phuntsho, I. El Saliby, H. K. Shon, Potential nutrient recovery from source-separated urine through hybrid membrane bioreactor and membrane capacitive deionisation, Desalination 566 (2023) 116924.
[14] F.J. Chu, N.N.N. Mahasti, B. Narindri Rara Winayu, The prospect of various applied methods for nutrient recovery in cattle wastewater: the case of precipitation, biological, and integrated method, J. Water Process Eng. 74 (2025) 107807.
[15] S.C. Motshekga, Nutrient recovery from wastewater using bioelectrochemical systems: a review on nitrogen and phosphorus removal, J. Water Process Eng. 79 (2025) 109031.
[16] Y. Yu, P. Perumal, T. Sithole, T. Luukkonen, Recovery of ammonium and nitrate from wastewater using adsorption-based techniques: a review, J. Clean. Prod. 519 (2025) 145976.
[17] L. Zhang, J. Liu, L. Yang, Z. Yu, J. Chen, H. Chu, Y. Zhang, X. Zhou, Interfacial solar evaporation toward efficient recovery of clean water and concentration of nutrients from urine with polypyrrole-based photothermal conversion films, Resour. Conserv. Recycl. 188 (2023) 106645.
[18] Z. Yao, Z. Li, X. Ao, M.R. Alizadeh, X. Zhou, S. Cheng, J.F. Adamowski, Unlocking ultralow-energy and high-efficiency urine resource recovery via solar-driven aerogel interfacial evaporation, Chem. Eng. J. 527 (2026) 171558.
[19] V. Koskue, S. Freguia, Coupling of urea hydrolysis, acetic acid fermentation and mineral precipitation during urine storage for nutrient recovery, J. Water Process Eng. 80 (2025) 109091.
[20] H. Wu, C. Vaneeckhaute, Nutrient recovery from wastewater: a review on the integrated physicochemical technologies of ammonia stripping, adsorption and struvite precipitation, Chem. Eng. J. 433 (2022) 133664.
[21] Y. Wang, H. Yu, X. Yang, L. Liu, S. Xu, H. He, Y. Zhang, T. He, Concentrating phosphoric acid by direct contact membrane distillation using a low-cost polyethylene separator, Desalination 530 (2022) 115664.
[22] A. Arkin, Z. Li, Membrane distillation for sustainable urine resource management: recovery potential and implementation challenges, Desalination 615 (2025) 119247.
[23] W.A.F. Wae AbdulKadir, R. Che Omar, M.H.Z. Mohd Harun, A.L. Ahmad, Innovative two-stage membrane distillation: a breakthrough in ammonia removal and recovery, Desalination 615 (2025) 119225.
[24] N. Thi My Hanh, N. Hong Van, P. Thi Minh Trang, Ammonium recovering from domestic wastewater toward circular economy: a short review, Desalin. Water Treat. 321 (2025) 100906.
[25] F. Wang, Y. Yang, J. Gao, X. Li, Z. Lu, X. Fan, S. Cao, Y. Liu, L.D. Tijing, H.K. Shon, J. Ren, Ultra-rapid start-up biological nitrification for nutrient recovery from source-separated urine, Water Res. 287 (2025) 124343.
[26] W.V. Macedo, J.S. Madsen, P. Schacksen, R. Sandeep, J.L. Nielsen, P. Biller, L. Vergeynst, Aerobic biological treatment of hydrothermal liquefaction process water of sewage sludge: nitrification inhibition and removal of hazardous pollutants, Water Res. 277 (2025) 123351.
[27] H.J. Qin, S. Ji, R. Wu, Y. Yamamoto, Y. Liu, B.S. Xing, Y. Qin, Y.Y. Li, Assessing biomass retention-driven enhancement of bioenergy and nutrient recovery potential in anaerobic membrane bioreactors for sustainable sewage sludge management, Bioresour. Technol. 437 (2025) 133105.
[28] Y.L. Yang, Y. Wu, Y.X. Lu, Y. Cai, Z. He, X.L. Yang, H.L. Song, A comprehensive review of nutrient-energy-water-solute recovery by hybrid osmotic membrane bioreactors, Bioresour. Technol. 320 (2021) 124300.
[29] M.S. Pourbavarsad, B.J. Jalalieh, N. Landes, W.A. Jackson, Impact of free ammonia and free nitrous acid on nitritation in membrane aerated bioreactors fed with high

strength nitrogen urine dominated wastewater, J. Environ. Chem. Eng. 10 (2022) 107001.
[30] W. Gao, Z. Wang, F. Duan, Y. Li, S. Shi, Z. Sun, B. Zhou, L. Lv, Comprehensive assessment of membrane technology for typical water treatment processes: a critical review, Desalination 614 (2025) 119171.
[31] R. Srivastava, A.K. Jaiswal, J. Swaminathan, Two-staged multi-effect distillation for energy efficient brine concentration, Desalination 600 (2025) 118511.
[32] P. Zheng, C. Guan, Z. Hao, P. Wang, X. Zhu, Y. Lv, P. Wang, X. Liu, Z. Song, G. Guo, Z. Hu, X. Liu, Z. Su, D. Zhao, S. Wang, Frontier research progress on the separation of source-separated urine by membrane distillation technology, Desalin. Water Treat. 325 (2026) 101623.
[33] B.M. An, S.L. Aung, J. Choi, H. Cha, J. Cho, B. Byambaa, K.G. Song, Behavior of solutes and membrane fouling in an electrodialysis to treat a side-stream: migration of ions, dissolved organics and micropollutants, Desalination 549 (2023) 116361.
[34] L. Shi, S. Xie, Z. Hu, G. Wu, L. Morrison, P. Croot, H. Hu, X. Zhan, Nutrient recovery from pig manure digestate using electrodialysis reversal: membrane fouling and feasibility of long-term operation, J. Membr. Sci. 573 (2019) 560–569.
[35] R. Mohammadi, W. Tang, M. Sillanpää, A systematic review and statistical analysis of nutrient recovery from municipal wastewater by electrodialysis, Desalination 498 (2021) 114626.
[36] S.L. Aung, J. Choi, H. Cha, G. Woo, K.G. Song, Ammonia-selective recovery from anaerobic digestate using electrochemical ammonia stripping combined with electrodialysis, Chem. Eng. J. 479 (2024) 147949.
[37] P. Genz, V.T. Katayama, T. Reemtsma, Retention of organic micropollutants in nutrient recovery from Centrate by Electrodialysis—influence of feed pH and current density, ACS EST Water 3 (12) (2023) 4066–4073.
[38] X. Pan, Y. Li, Y. Huang, J. Xu, C. Sun, Z.-L. Ye, Electrodialysis, a promising approach for nutrients recovery from anaerobic liquid digestate: status, challenges and perspectives, J. Water Process Eng. 72 (2025) 107658.
[39] P. Ruiz-Barriga, S. Hernández-Cuenca, J. Serralta, R. Barat, A. Bouzas, J. Carrillo-Abad, Long-term electrodialysis nutrient concentration from anaerobic membrane bioreactor effluents: challenges for calcium sulfate precipitation, Desalination 626 (2026) 119969.
[40] H.R. Yang, Y. Liu, S.J. Hu, M.Y. Zhang, D. Wu, L. Zheng, L.J. Zhong, C. Wang, H. Liu, Advanced electrochemical membrane technologies for near-complete resource recovery and zero-discharge of urine: performance optimization and evaluation, Water Res. 263 (2024) 122175.
[41] H. Yu, G. Naidu, C. Zhang, C. Wang, A. Razmjou, D.S. Han, T. He, H. Shon, Metal-based adsorbents for lithium recovery from aqueous resources, Desalination 539 (2022) 115951.
[42] C. Morgante, M. Herrero-Gonzalez, J. Lopez, J. Imholze, V. Boffa, R. Ibañez, J. L. Cortina, A global outlook of the desalination industry and state-of-the-art technologies for brine valorisation, Desalination 621 (2026) 119718.
[43] M. Tahmid, H. Joo Choi, S.T. Ganapavarapu, J. Scott, M.C. Hatzell, Concentrating nitrogen waste with Electrodialysis for fertilizer production, Environ. Sci. Technol. Lett. 11 (12) (2024) 1413–1419.
[44] N. Pathak, H. Shon, H. Yu, Y. Choo, G. Naidu, N. Akther, D.-S. Han, Membrane technology for brine management and valuable resource recovery, in: Green Membrane Technologies towards Environmental Sustainability, 2023, pp. 415–441.
[45] J. De Paepe, R.E.F. Lindeboom, M. Vanoppen, K. De Paepe, D. Demey, W. Coessens, B. Lamaze, A.R.D. Verliefde, P. Clauwaert, S.E. Vlaeminck, Refinery and concentration of nutrients from urine with electrodialysis enabled by upstream precipitation and nitrification, Water Res. 144 (2018) 76–86.
[46] D. Poitras, V. Perreault, S. Gaaloul, P. Schuck, L. Bazinet, Lactic acid removal and demineralization of acid whey by coupling electrodialysis under pulsed electric fields with pre-concentration by nanofiltration: impact on spray drying and powder quality, Desalination 613 (2025) 119032.
[47] P. Ruiz-Barriga, J. Serralta, A. Bouzas, J. Carrillo-Abad, Boosting nutrient recovery from AnMBR effluent by means of electrodialysis technology: operating parameters assessing, J. Environ. Manage. 366 (2024) 121712.
[48] Z.L. Ye, K. Ghyselbrecht, A. Monballiu, L. Pinoy, B. Meesschaert, Fractionating various nutrient ions for resource recovery from swine wastewater using simultaneous anionic and cationic selective-electrodialysis, Water Res. 160 (2019) 424–434.
[49] A.J. Ward, K. Arola, E. Thompson Brewster, C.M. Mehta, D.J. Batstone, Nutrient recovery from wastewater through pilot scale electrodialysis, Water Res. 135 (2018) 57–65.
[50] V. Proskynitopoulou, A. Vourros, P. Dimopoulos Toursidis, I. Garagounis, S. Lorentzou, M. Bampaou, K. Plakas, A. Zouboulis, K. Panopoulos, Selective electrodialysis for nutrient recovery and pharmaceutical removal from liquid digestate: pilot-scale investigation and potential fertilizer production, Bioresour. Technol. 412 (2024) 131386.
[51] F. Kotoka, L. Gutierrez, A. Verliefde, E. Cornelissen, Selective separation of nutrients and volatile fatty acids from food wastes using electrodialysis and membrane contactor for resource valorization, J. Environ. Manage. 354 (2024) 120290.
[52] J. Meng, L. Shi, W. Bai, Z. Hu, L. Zhen, A. Terada, X. Zhan, P. Crosson, Application of electrodialysis for nutrient recovery from manure digestate: a long-term investigation of membrane fouling, Water Res. X 29 (2025) 100420.
[53] V. Koskue, S. Freguia, P. Ledezma, M. Kokko, Efficient nitrogen removal and recovery from real digested sewage sludge reject water through electroconcentration, J. Environ. Chem. Eng. 9 (2021) 106286.
[54] A.T.K. Tran, Y. Zhang, J. Lin, P. Mondal, W. Ye, B. Meesschaert, L. Pinoy, B. Van der Bruggen, Phosphate pre-concentration from municipal wastewater by selectrodialysis: effect of competing components, Sep. Purif. Technol. 141 (2015) 38–47.
[55] B. Meesschaert, K. Ghyselbrecht, A. Monballiu, L. Pinoy, Pilot scale anion selectrodialysis for water reclamation and nutrient recovery from UASB effluent after nitrification, ultrafiltration and UV C treatment, Environ. Technol. Innov. 22 (2021) 101449.
[56] R. Mohammadi, D.L. Ramasamy, M. Sillanpää, Enhancement of nitrate removal and recovery from municipal wastewater through single- and multi-batch electrodialysis: process optimisation and energy consumption, Desalination 498 (2021) 114726.
[57] S.-Y. Pan, J.M. Gianto, Y.-I. Lin, H.-M. Chang, Advancing water and resource recovery from brackish water through electrodialysis-based technologies for circular product ecosystems, Desalination 619 (2026) 119550.
[58] A. Lugo, M.F. Ahmed, T.L. Oddonetto, P.S. Senanayake, I. Basnayake, Z. Stoll, M. Ehsani, N.E. Moe, J. Barber, H. Wang, P. Xu, Operational optimization of bipolar membrane electrodialysis for acid and base production in zero liquid discharge of high-salinity brine, Desalination 615 (2025) 119290.
[59] A. Anwar, S. Ates, B. Yuzer, Y. Bicer, Exploring the potential of single-batch and multi-batch electrodialysis treatment of domestic wastewater for resource recovery, J. Environ. Manage. 394 (2025) 127209.
[60] Z. Dai, C. Chen, Y. Li, H. Zhang, J. Yao, M. Rodrigues, P. Kuntke, L. Han, Hybrid Donnan dialysis-electrodialysis for efficient ammonia recovery from anaerobic digester effluent, Environ Sci Ecotechnol 15 (2023) 100255.
[61] Y. Li, Z.L. Ye, R. Yang, S. Chen, Synchronously recovering different nutrient ions from wastewater by using selective electrodialysis, Water Sci. Technol. 86 (10) (2022) 2627–2641.
[62] Y. Zhang, E. Desmidt, A. Van Looveren, L. Pinoy, B. Meesschaert, B. Van der Bruggen, Phosphate separation and recovery from wastewater by novel electrodialysis, Environ. Sci. Technol. 47 (11) (2013) 5888–5895.
[63] W. Sohn, A. Merenda, A.H. Shafaghat, I. El Saliby, Y. Zhang, X. Jia, J. Guan, S. Phuntsho, H.K. Shon, Influence of temperature and dissolved oxygen on nitrification in a membrane bioreactor treating urine, J. Water Process Eng. 78 (2025) 108721.
[64] J. Park, J. Lee, I.-T. Shim, E. Kim, S.-H. Nam, J.-W. Koo, T.-M. Hwang, Electrochemical direct lithium extraction: a review of electrodialysis and capacitive deionization technologies, Resources 14 (2) (2025).
[65] I. Atlas, J. Wu, A.N. Shocron, M.E. Suss, Spatial variations of pH in electrodialysis stacks: theory, Electrochim. Acta 413 (2022) 140151.
[66] V.D. Ruleva, K.V. Brizhan, N.D. Pismenskaya, M.A. Ponomar, M.V. Sharafan, K. G. Sabbatovskiy, C. Jiang, Y. Wang, T. Xu, V.V. Nikonenko, Impact of membrane and electrolyte properties on the intensity of equilibrium electroconvection in electrodialysis, J. Membr. Sci. 741 (2026) 125004.
[67] E. Thompson Brewster, J. Jermakka, S. Freguia, D.J. Batstone, Modelling recovery of ammonium from urine by electro-concentration in a 3-chamber cell, Water Res. 124 (2017) 210–218.
[68] S.M. Hossain, H. Yu, Y. Choo, G. Naidu, D.S. Han, H.K. Shon, ZiF-8 induced carbon electrodes for selective lithium recovery from aqueous feed water by employing capacitive deionization system, Desalination 546 (2023) 116201.
[69] H. Yu, S.M. Hossain, C. Wang, Y. Choo, G. Naidu, D.S. Han, H.K. Shon, Selective lithium extraction from diluted binary solutions using metal-organic frameworks (MOF)-based membrane capacitive deionization (MCDI), Desalination 556 (2023) 116569.
[70] T. Luo, S. Abdu, M. Wessling, Selectivity of ion exchange membranes: a review, J. Membr. Sci. 555 (2018) 429–454.
[71] S. Xu, R. He, C. Dong, N. Sun, S. Zhao, H. He, H. Yu, Y.-B. Zhang, T. He, Acid stable layer-by-layer nanofiltration membranes for phosphoric acid purification, J. Membr. Sci. 644 (2022) 120090.
[72] H. Yu, M.J. Park, C. Wang, D. Liang, T. He, G. Naidu, D.S. Han, H.K. Shon, Integrated sulfonated poly ether ketone membrane capacitive deionization for lithium recovery from diluted binary solutions, Sep. Purif. Technol. 352 (2025) 128064.
[73] C. Wang, M.J. Park, H. Yu, H. Matsuyama, E. Drioli, H.K. Shon, Recent advances of nanocomposite membranes using layer-by-layer assembly, J. Membr. Sci. 661 (2022) 120926.
[74] H. Yu, C. Wang, S. Phuntsho, T. He, G. Naidu, D.S. Han, H.K. Shon, Highly selective lithium recovery from seawater desalination brine using Li(2)TiO(3) membrane-coated capacitive deionization, Water Res. 285 (2025) 124113.
[75] H. Yu, S. Phuntsho, G. Naidu, M. Askari, H.K. Shon, Advances in capacitive deionization for selective lithium recovery from brines: mechanisms, strategies, and future perspectives, Desalination 629 (2026) 120098.
[76] W. Zhai, H. Yu, H. Chen, L. Li, D. Li, Y. Zhang, T. He, Stable fouling resistance of polyethylene (PE) separator membrane via oxygen plasma plus zwitterion grafting, Sep. Purif. Technol. 293 (2022) 121091.
[77] C. Wang, L. Wang, H. Yu, A. Seo, Z. Wang, S. Rajabzadeh, B.J. Ni, H.K. Shon, Machine learning for layer-by-layer nanofiltration membrane performance prediction and polymer candidate exploration, Chemosphere 350 (2024) 140999.
[78] N. Pismenskaya, A. Gorobchenko, K. Solonchenko, V. Nikonenko, Effect of current density on anion-exchange membrane scaling during electrodialysis of phosphate-containing solution: experimental study and predictive simulation, Desalination 600 (2025) 118487.
[79] Z. Jia, C. Liu, M. Tan, F. Liu, W. Cong, R. Fu, Y. Liu, Y. Zhang, Proton and water migration regulation drives high-efficiency sulfuric acid concentration via ladder electrodialysis, Desalination 620 (2026) 119663.
[80] Q. Chen, J. Shan, Z. Chen, L. Ge, T. Xu, Water transport engineering in electrodialysis: a pathway to efficient lithium extraction from high Mg/Li ratio brines, Desalination 622 (2026) 119764.

[81] M. Roman, L. Gutierrez, L.H. Van Dijk, M. Vanoppen, J.W. Post, B.A. Wols, E. R. Cornelissen, A.R.D. Verliefde, Effect of pH on the transport and adsorption of organic micropollutants in ion-exchange membranes in electrodialysis-based desalination, Sep. Purif. Technol. 252 (2020) 117487.
[82] L. Marder, S.D. Bittencourt, J. Zoppas Ferreira, A.M. Bernardes, Treatment of molybdate solutions by electrodialysis: the effect of pH and current density on ions transport behavior, Sep. Purif. Technol. 167 (2016) 32–36.
[83] C.Y. Wei, S.Y. Pan, Y.I. Lin, T.N. Cao, Anaerobic swine digestate valorization via energy-efficient electrodialysis for nutrient recovery and water reclamation, Water Res. 224 (2022) 119066.
[84] H.J. Choi, M. Tahmid, S. Mondal, M.C. Hatzell, Concentrating ammonia from wastewater with electrodialysis, ACS EST Water 5 (9) (2025) 5720–5727.